Lithos 384–385 (2021) 105940

Contents lists available at ScienceDirect

Lithos

journal homepage: www.elsevier.com/locate/lithos

Research Article

Prolonged magmatism and growth of the Iran-Anatolia Cadomian continental arc segment in Northern Gondwana

H. Shafaii Moghadam [a,b,c,d,*], Q.L. Li [b,*], W.L. Griffin [d], R.J. Stern [e], J.F. Santos [f], F. Lucci [g], M. Beyarslan [h], G. Ghorbani [a], A. Ravankhah [i], R. Tilhac [j], S.Y. O'Reilly [d]

[a] School of Earth Sciences, Damghan University, Damghan 36716-41167, Iran
[b] State Key Laboratory of Lithospheric Evolution, Institute of Geology and Geophysics, Chinese Academy of Sciences, Beijing 100029, China
[c] FB4-Dynamics of the Ocean Floor, GEOMAR, Helmholtz-Zentrumfür Ozeanforschung Kiel, Wischhofstr. 1-3, 24148 Kiel, Germany
[d] CCFS & GEMOC ARC National Key Centre, Macquarie University, NSW 2109, Australia
[e] Geosciences Dept. University of Texas at Dallas, Richardson, TX 75083-0688, USA
[f] Geobiotec., Departamento de Geociências, Universidade de Aveiro, 3810-193 Aveiro, Portugal
[g] Dipartimento di Scienze, Università "Roma Tre", 00146 Rome, Italy
[h] Firat University, Dept. of Geological Engineering, Turkey
[i] Department of Geology, Faculty of Sciences, University of Mohaghegh Ardabili, Ardabil 56199-13131, Iran
[i] Instituto Andaluz de Ciencias de la Tierra (IACT), CSIC – Universidad de Granada, 18100 Armilla, Granada, Spain

ARTICLE INFO

Article history:
Received 24 September 2020
Received in revised form 15 December 2020
Accepted 15 December 2020
Available online 19 December 2020

Keywords:
Cadomian magmatism
Arc-like igneous rocks
Magmatic flare-up
Back-arc
Anatolia
Iran

ABSTRACT

Much of the crust of Iran and Anatolia, including their oldest exposed rocks, formed during an episode of intense convergent margin (arc) magmatism as a result of subduction of oceanic lithosphere beneath northern Gondwana from *ca* 620 Ma to *ca* 500 Ma, the Cadomian crust-forming event. Most igneous rocks formed between *ca* 570 and 525 Ma. Cadomian crust is well-known from western and southern Europe and from eastern North America but is much less well-known from Iran and Anatolia. We use published age and compositional data and contribute new data in order to better understand this ancient magmatic system. Cadomian magmatism included calc-alkaline igneous rocks of arc affinity in the main arc and alkalic igneous rocks that formed in a back-arc setting; these igneous rocks are associated with sedimentary rocks. Geochemical and isotopic modelling reveals that basaltic magmas were the main input, that these formed by partial melting in the upper mantle, and that basaltic magmas evolved further in deep crustal hot zones to form granitic magmas through a combination of assimilating older continental crust and fractional crystalization of basaltic magmas.

1. Introduction

Continental arcs are regions with high magmatic flux above subduction zones and are important sites of crustal growth and reworking. Fossilized continental arcs are especially useful because both upper volcanic and lower plutonic parts can be examined. These provide especially useful insights for examining crustal growth processes because moderate erosion exposes a record of arc evolution that cannot be accessed by studies of active arcs. Studies of fossilized continental arcs such as the western North America cordillera indicate that arc magmatism is episodic, characterized by 20–30 Ma episodes of high magmatic flux or "flare-up" separated by longer magmatic lulls when less magma is produced (Ducea and Barton, 2007). Flare-ups represent major pulses of crust formation and reworking.

The Cadomian crust offers a good opportunity to study the record of Late Neoproterozoic-Early Cambrian crust formation and reworking associated with arc magmatism in northern Gondwana. This was the second episode of arc magmatism that affected Gondwana in Neoproterozoic and Early Cambrian time. Intense Neoproterozoic magmatism generated much juvenile crust, especially in the Arabian-Nubian Shield (ANS) and also reworked older crust to the west, in the Saharan Metacraton (Abdelsalam et al., 2002), as well as to the northwest of the ANS, in the Eastern Desert (Li et al., 2018). This episode is marked by Tonian and Cryogenian arc magmatism, followed by Ediacaran collisional and post-collisional magmatism, ultimately welding the Greater Gondwana supercontinent together. As this supercontinent cycle ended at ~600 Ma, a new subduction system formed along the northern margin of the supercontinent and a new magmatic arc was established in Ediacaran-Early Cambrian time (620–500 Ma). Igneous

* Corresponding authors at: School of Earth Sciences, Damghan University, Damghan 36716-41167, Iran (Hadi Shafaii Moghadam) and State Key Laboratory of Lithospheric Evolution, Institute of Geology and Geophysics, Chinese Academy of Sciences, Beijing 100029, China (Qiu-li Li)
E-mail addresses: hadishafaii@du.ac.ir (H.S. Moghadam), liqiuli@mail.iggcas.ac.cn (Q.L. Li).

https://doi.org/10.1016/j.lithos.2020.105940
0024-4937/

rocks and sediments generated during this episode, referred to as the Cadomian, make up much of the crust of Western Europe; some western segments are called Avalonian. Cadomian and Avalonian crust now underlies large tracts of eastern North America, southern and central Europe, Iran and Turkey. Cadomian magmatic, sedimentary and metamorphic rocks dominate the basement of Europe, southwest of the Baltic craton, including Iberia, Armorica and Bohemia (Linnemann et al., 2011; Tilhac et al., 2017). Cadomian crust can be traced eastwards into southeast Europe, Iran and Anatolia, and perhaps further into Central Asia (von Raumer et al., 2002).

The Cadomian-Avalonian magmatic arc formed during the subduction of Prototethys beneath northern Gondwana, as evidenced by the presence of Ediacaran high-P rocks, ophiolites and accreted arc complexes (*e.g.*, (Triantafyllou et al., 2020)) (Fig. 1A). Magmatism began ~620 Ma and ended ~500 Ma, although most activity occurred between 570 and 530 Ma. This single continental magmatic arc broke into fragments that rifted away during the Paleozoic and Mesozoic to open the Rheic and Paleotethys Oceans (Nance et al., 2002), and eventually accreted to southern Laurasia. Recent studies of U–Pb ages and Hf-isotopes in zircon have addressed the age and geochemical evolution of Cadomian magmatic rocks in western and southern Europe as well as the provenance of Cadomian sedimentary rocks (*e.g.*, (Abbo et al., 2015; Avigad et al., 2015)). Although Cadomian magmatic rocks in Europe are well characterized, Cadomian magmatism in Iran and Anatolia is less well known. This paper reports new and compiled bulk rock Sr–Nd and zircon U–Pb and Lu–Hf isotopic data for Cadomian magmatic rocks from Iran and Anatolia. This is an enormous tract of continental crust, almost 3000 km long and hundreds of kilometers wide. We use these data to estimate rates of magmatic addition and to constrain how the source associated with the Cadomian magmatism of Iran and Anatolia evolved. We also discuss tectonic and magmatic mechanisms and their roles in controlling magmatic activity during the evolution of this part of the great Cadomian-Avalonian magmatic arc.

2. Cadomian crust of Iran and Anatolia

It is not known precisely where the Cadomian magmatic rocks of Iran and Anatolia formed, but this probably was somewhere on the northern flank of the present-day Arabian-Nubian Shield (ANS) and eastern Arabia (EA) and perhaps adjacent to the Saharan Metacraton further west (Fig. 1A). ANS tectono-magmatic evolution began ~880 Ma as intra-oceanic convergent margins and ended at 570 Ma as colliding blocks of East and West Gondwana were joined along the East African Orogen (-EAO). Most eastern Arabia magmatic activity occurred between ~900 and 750 Ma (Stern and Johnson, 2010). We know little about the Saharan Metacraton but this crust seems to include important elements of Neoarchean and Paleoproterozoic crust that was intensely reworked by pervasive Ediacaran magmatism.

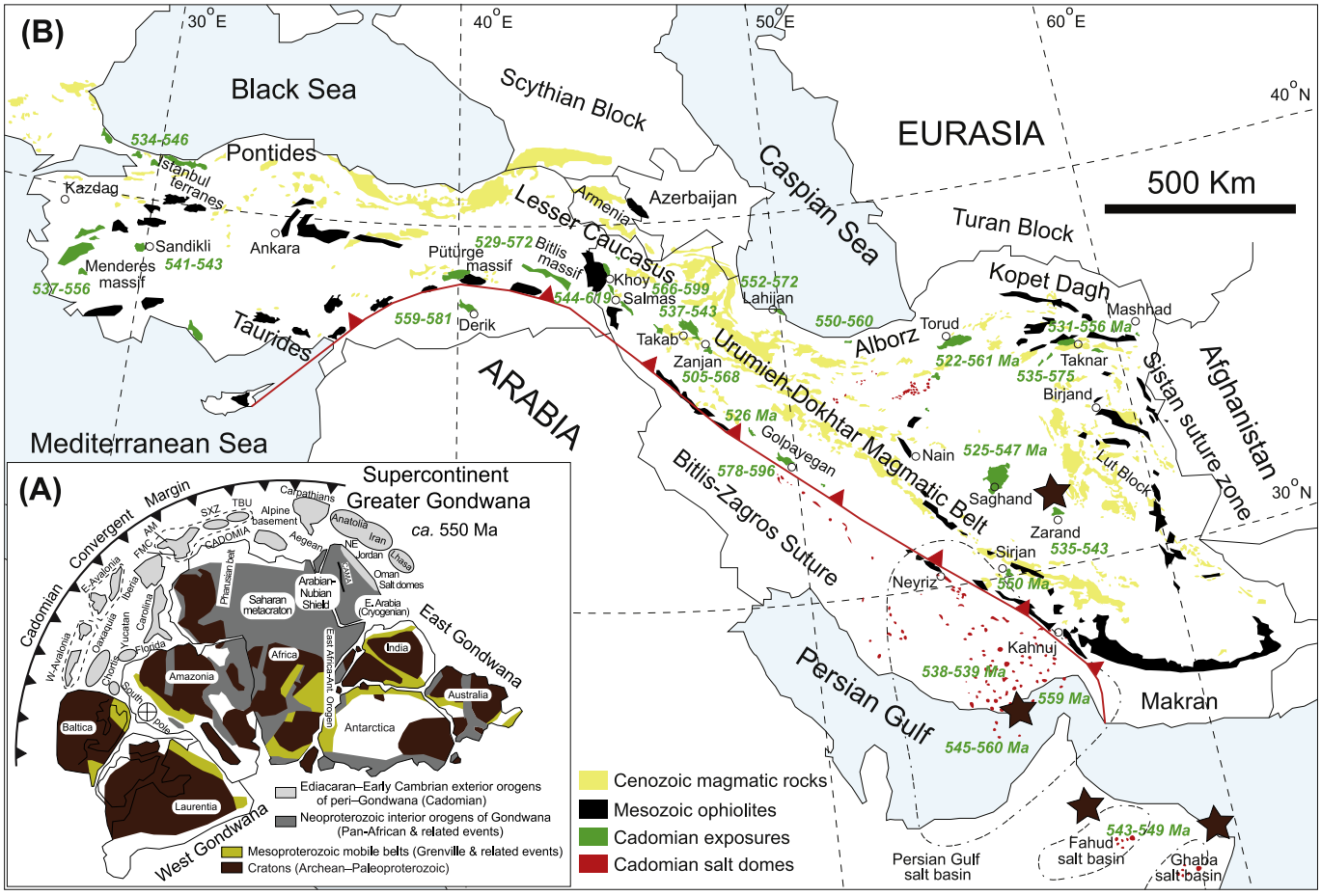

Fig. 1. A- Paleogeography of the Cadomian-Avalonian active margin and related major peri-Gondwanan terranes at ~550 Ma (modified after (Linnemann et al., 2010)). AM = Armorian massif, FMC=French massif central, SXZ = Saxo-Thuringian zone (part of the Bohemian massif), TBU = Tepla-Barrandian Unit (part of the Bohemian massif). B- Simplified geological map of Iran- Turkey showing the distribution of Cenozoic igneous rocks, Paleozoic-Mesozoic ophiolites and the Cadomian basement rocks and salt domes. Brown starts show the location of alkaline (anorogenic) rocks which are associated with thick sequence of terrigenous sedimentary rocks and evaporites.

Magmatic activity along the Cadomian arc segment of Iran and Anatolia was diachronous- since they have been formed in an identical subduction-related tectono-magmatic setting, but through different time. Despite the whole setting was subduction-related, but magmatism was also accompanied by the extension in the overlying plate. The extensional setting is inferred by abundant Cadomian volcano-sedimentary basins, including back-arc or rear-arc basins that widened after ~530 Ma to form the Rheic Ocean (Linnemann et al., 2014). Opening of these basins also led to the Early Paleozoic rifting of Gondwana at ~490 to 480 Ma to open Paleotethys (Moghadam et al., 2017b; Nance et al., 2010) (Fig. 2). Broad tracts of the Cadomian continental arc including the Cadomian crust of Iran and Anatolia accreted to south Eurasia as the result of Permian-Early Triassic opening (Moghadam et al., 2015) and Late Mesozoic closure of Neotethys (Topuz et al., 2013). These Cadomian terranes are now dominated by meta-sedimentary and meta-igneous rocks and magmatic exposures are particularly widespread in Iran (Fig. 1B). Exposures are also scattered across Turkey, in the east (Bitlis-Pütürge massifs), west (Menderes-Sandikli) and NW (Istanbul zone; Fig. 1B). The Cadomian basement of Iran and Anatolia was mostly exhumed as a result of Cenozoic extension.

Cadomian arc crust exposed in Iran and Anatolia consists of a heterogeneous assemblage of magmatic rocks with different types of occurrence, lithology and geochemical signatures. It is dominated by felsic plutons along with minor acidic extrusive rocks. Mafic magmatic rocks are less abundant (Fig. 3). There are several main exposures.

(a) Calc-alkaline metagranites to metagabbros associated with mafic to felsic ortho-gneisses associated with subordinate mafic and felsic volcanic rocks. These are exposed in the Bitlis-Pütürge and Menderes-Sandikli massifs in Anatolia and comprise nearly all Cadomian exposures in Iran (Fig. 1B). Paragneisses, metapsammites and metapelites (metamorphosed in upper greenschist to upper amphibolite facies) with rare granulites are closely associated with these rocks (Nutman et al., 2014; Ustaomer et al., 2009). Significant amounts of metamorphosed terrigenous sediments (psammitic paragneisses) are present; these were mostly (>90%) derived from erosion of local Cadomian rocks (both sedimentary and magmatic rocks) and deposited in intra-arc and back-arc basins (Balaghi Einalou et al., 2014; Moghadam et al., 2017b). The maximum age of sedimentation is variable and overlaps with the local magmatism. Due to exhumation from the middle crust, most of the Cadomian magmatic and metamorphic rocks are deformed and some have undergone partial melting and migmatization. Felsic rocks include arc-related I-type magmatic rocks with less abundant A-type (A_2-type) granites and rhyolites, which are interpreted to have formed in a rear-arc environment. Metamorphosed dikes (now orthogneisses) are present. Muscovite-bearing S-type granites are rare but occur in northwest Iran (Shahzeidi et al., 2017) and the Menderes massif of Taurids (Erkül and Erkül, 2012)), although their isotopic signatures indicate these S-type granites are not pure melts of upper crust sediments.

(b) Unmetamorphosed mafic to felsic volcanic rocks and dikes/sills reflecting mostly bimodal magmatism. Such bimodal magmatism is known from magmatic arcs elsewhere. These rocks are reported from near Zarand-Saghand in central Iran and as exotic blocks in Ediacaran salt domes in southeast Iran, the north UAE and northeast Oman (Sepidbar et al., 2020). These rocks show calc-alkaline I-type and A-type (anorogenic) signatures and are associated with thick (>1000 m) terrigenous sedimentary rocks, evaporites and dolomites known as the Morad and Rizu-Dezu series in southeast and Central Iran, the Hormoz series in southeast Iran and the Ara group in Oman. These metasediments are also stratigraphic equivalents of the Tashk and Kahar volcano-sedimentary (with glacio-sediments) formations (with ages of 550–520 Ma) from central Iran (Saghand) and north Iran, respectively (Etemad-Saeed et al., 2015; Ramezani and Tucker, 2003). The Derik complex in northern margin of the Arabian plate also contains andesites and rhyolites intercalated with Cadomian volcanic breccias. The volcanic sequence is crosscut by basaltic dikes. Zircon U–Pb dating of andesites and rhyolites indicates ages of 559 to 581 Ma (Gursu et al., 2015).

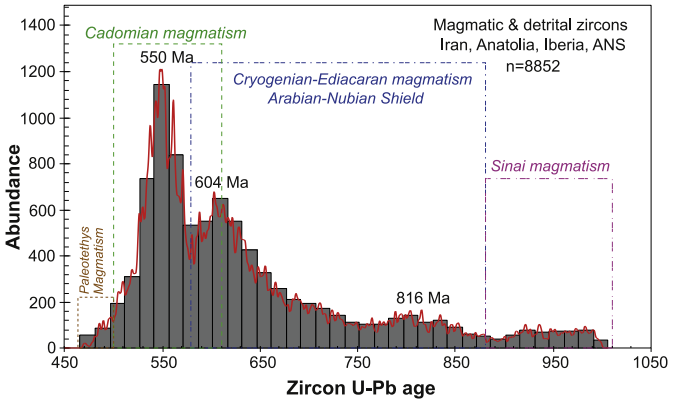

Fig. 2. Probability diagrams for $^{206}Pb/^{238}U$ ages ($n = 8852$) of magmatic (both felsic and mafic rocks with SiO_2 ranging from 50 to 70 *wt%*) and detrital zircons from Iran, Anatolia, Iberia and ANS, showing the main magmatic events in northern Gondwana during Tonian, Cryogenian-Ediacaran, Cadomian and Early Paleozoic (see caption Fig. 4 in "Appendix A" for references).

Salt domes are unique to the Cadomian sedimentary basins around the eastern Persian Gulf in southeast Iran, the UAE, and northeast Oman (Fig. 1B). They include various type of exotic magmatic and sedimentary clasts set in a diapiric matrix of Ediacaran-Cambrian carbonates, green tuffs, red sandstone-siltstone beds, sodium and potash-rich salts, anhydrites and gypsum. Felsic exotic blocks from salt domes have yielded zircon U–Pb ages of 558 ± 7 Ma for the Hormuz series (Faramarzi et al., 2015), 560–545 Ma for exotic blocks in the salt domes of the north UAE and northeast Oman (Thomas et al., 2015), and 543 to 549 Ma for ignimbrites and rhyolites from the Oman salt basins (Bowring et al., 2007) (Fig. 1A). It is believed that these terrigenous sedimentary rocks and evaporites were deposited in an extensional back-arc basin on the landward side of the continental arc, and thus the terrigenous sedimentary rocks contain abundant Archean as well as Neoproterozoic (2.5 to 0.6 Ga) detrital zircons (Bowring et al., 2007).

(c) Some exposures from Central Iran (Saghand) and north Iran (in Alborz) contain A-type rhyolites, altered andesites, rhyolitic tuffs and spillitized basalts and dolerites with thick sequences of diamictites and cap carbonates. These central Iranian outcrops are also accompanied by glaciogenic (iron-apatite-bearing) banded iron formations and ash beds (Mohseni and Aftabi, 2015). These rocks have been dated to 635–515 Ma based on Pb isotope dating of galena, monazite and apatite (Stosch et al., 2011), but these ages have high uncertainties and the sedimentary sequences need to be dated with zircons from tuff layers. In Alborz, diamictites are associated with >2000 m of siliciclastic rocks and minor carbonates with zircon U–Pb depositional ages of 560–550 Ma (Etemad-Saeed et al., 2015); this is a bit younger than the ~580 Ma Gaskiers Snowball Earth episode (Pu et al., 2016), providing another promising avenue of future research.

(d) Exposures from northeast Iran include ultramafic-mafic hydrous, garnet-bearing cumulates similar to mafic granulites (with zircon U–Pb ages of 547–532 Ma for mafic rocks) which show evidence of forming in a deep crustal "hot zone" and foundering of lower-crustal cumulates (Moghadam et al., 2020a). Similar

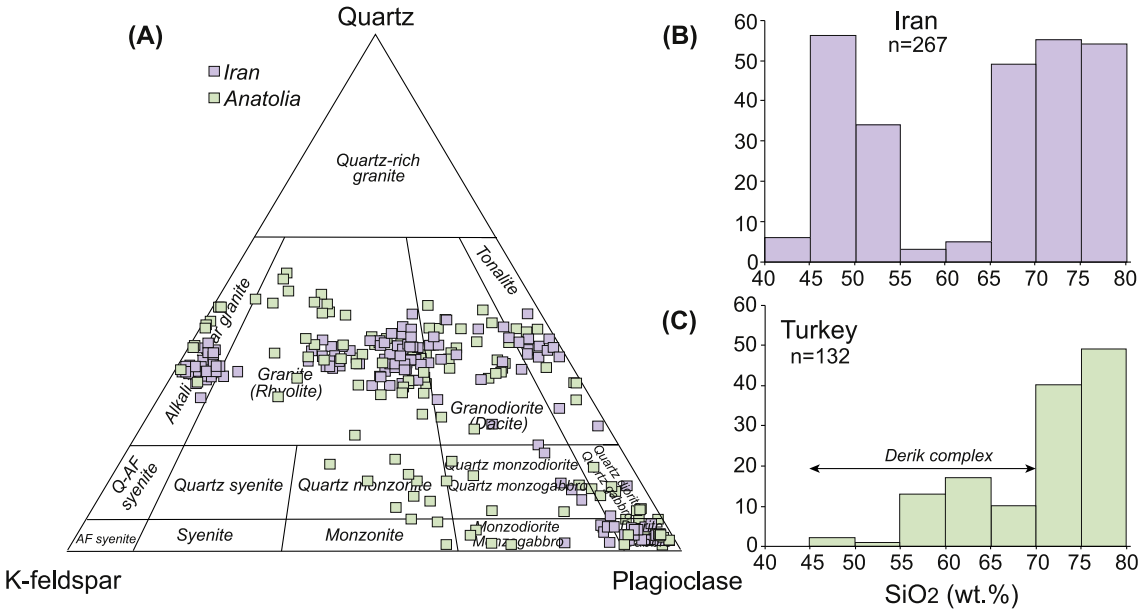

Fig. 3. A- Quartz-alkali feldspar-plagioclase (QAP) diagram for the modal classification of Iran and Anatolia Cadomian igneous rocks. B- and C- Bulk rock SiO_2 concentration histograms of the Cadomian magmatic pulses from Iran and Anatolia. See Tables S2A and S2B for references.

cumulates are present in other parts of the Cadomian arc, *e.g.*, in Iberia (Tilhac et al., 2016), but are not yet reported in Anatolia.

(e) It is unclear if Cadomian ophiolites exist in Iran and Anatolia. Some outcrops in Iberia and Anatolia include ophiolites and eclogites which are remnants of the Prototethys and Rheic oceans (Beyarslan et al., 2016; Candan et al., 2016); younger ophiolites (~ < 600 to 500 Ma) may be remnants of the Rheic ocean, whereas older ophiolites (~600 Ma) may be related to initiation of the Cadomian subduction zone within Prototethys (von Raumer et al., 2015). Cadomian exposures from northwest Iran contain metamorphosed sandstones, metagraywackes and metapelites associated with tectonic slices and blocks of serpentinites and metaperidotites (Saki et al., 2011), which may be fragments of Cadomian subduction zone-related ophiolites and associated accretionary prism, but precise ages are needed to test this idea. In central Iran there is a noticeable unconformity between Ediacaran-Early Cambrian sedimentary and igneous rocks and Mid-Late Cambrian siltstones, sandstones, conglomerates and cherty limestones.

2.1. Samples and methods

We consider three types of data.

(a) New and compiled zircon U–Pb ages and Lu–Hf isotopes for Cadomian magmatic rocks from northwest, southeast and central Iran as well as the Pütürge massif of Anatolia and some compiled data - mostly our own - on Cadomian Iran and Anatolian arcs as well as Cadomian xenoliths from salt domes in Iran and Oman. Our new samples include metagranites and granitic augen gneisses from the Pütürge massif and basalts-rhyolites and granites to gabbros as well as granitic to dioritic orthogneisses from Central (Saghand and Zarand) and NW Iran. Zircon U–Pb dating for new samples was carried out using both Cameca IMS-1280/HR SIMS and Laser Ablation Inductively Coupled Plasma-Mass Spectrometry (LA-ICPMS). Zircons have been further analysed for Lu–Hf using a laser ablation attached to a multicollector-inductively coupled plasma-mass spectrometer (LA-MC-ICPMS). Detailed analytical procedures can be found in "Appendix A" and the complete analytical data are given in Tables S1 to S6. GPS coordination data for the new analysed samples is presented in Table S7.

(b) New and compiled bulk-rock geochemical (major- and trace elements) and isotopic (Sr–Nd) data on mafic to felsic magmatic lithologies from Iran and Anatolia Cadomian arc and Iran-Oman salt domes. New samples were analysed for major and trace elements using X-Ray Fluorescence, Inductively Coupled Plasma-Atomic Emission Spectrometry (ICP-AES) and Inductively Coupled Plasma- Mass Spectrometry (ICP-MS). Sr and Nd analyses were performed using Multi-Collector Thermal Ionization Mass Spectrometer (TIMS). Analytical facilities used for these analyses are described in Appendix A. Our new and compiled data reveal compositions that vary from gabbro to granite (and basalt to rhyolite) to alkali-feldspar granites (A-type granites) in QAP modal diagram (Fig. 3).

(c) Compiled detrital zircon U–Pb ages and Lu–Hf isotopic data from Cadomian and Early-Mid Paleozoic terrigenous rocks of Iran and Anatolia. To compare our Cadomian data with the Cryogenian-Cadomian magmatism of the ANS and Iberia, we also have compiled data on magmatic and detrital zircon U-Pb-Hf from the ANS and Iberia.

3. Results

3.1. Age of magmatic pulses

We have analysed new samples and gathered zircon U–Pb data published on magmatic and detrital zircons from nearly all Cadomian outcrops of Iran and Anatolia to avoid sampling bias. We used magmatic zircons (*e.g.*, with oscillatory zoning and Th/U > 0.1) and avoided zircon rims (which were rare). We infer that the zircon U–Pb data from each magmatic sample represents the best estimate of the emplacement age of arc magmatic intrusions and/or eruption of volcanic rocks. The compilation of zircon U–Pb data indicates that the magmatism in the ANS and Cadomia lasted over ~370 Myr (850–480 Ma; Fig. 2). These data imply that magmatic activity was continuous but with three

main events represented by peaks of zircon ages. These are described as periods of high magma flux at 850–750 Ma (with peak at 816 Ma), 750–590 Ma (with peak at 604 Ma) and 570–510 Ma (with peak at 550 Ma) interrupted by periods of less magmatic activity. The older magmatism of 850 to 590 was connected to the ANS juvenile magmatism, which was triggered by continental and oceanic arc magmatic activities as well as during the amalgamation of continental fragments, whereas the younger cycle was related to the Cadomian magmatism.

U–Pb magmatic zircon ages from Iran and Anatolia indicate that Cadomian magmatism took place between 600 and 500 Ma and was especially intense during a 45-Myr timespan *ca* 570–525 Ma in Iran and Anatolia (Fig. 4A–C), in good agreement with detrital zircon data from Cadomian and Paleozoic strata of Iran and Anatolia (*e.g.*, (Abbo et al., 2015; Avigad et al., 2015), but quite different from our compiled detrital zircon dataset (see next section). New zircon data reported here also show that magmatism probably started earlier in NW Iran, at ~619 ± 6.5 Ma, and at ~630 ± 20 Ma in central Iran (Nutman et al., 2014). Felsic and mafic magmatic episodes are coeval but felsic igneous rocks are more abundant (Fig. 3B–C). Early Cadomian magmatism overlaps with post-collisional (Ediacaran) juvenile magmatism in the ANS at >580 Ma. Late Cadomian magmatism overlaps with Early Paleozoic magmatism (<500 Ma) linked to the opening of the Rheic and Paleotethys oceans.

3.2. Geochemical significance of the Cadomian magmatic rocks

In order to study the geochemical evolution of Cadomian magmatic rocks we also compiled all bulk rock data for magmatic rocks of Iran and Anatolia (with a few additional new samples reported in Table S8). Since our new and compiled geochemical data come from a long Cadomian belt of Iran and Anatolia, which is represented by ~100 Myr magmatic activities, there might be a spatial and temporal differences between analysed samples. Considering this, we have classified our samples according their location (Iran *vs* Anatolia), their composition (*e.g.*, felsic *vs* mafic) and their tectono-magmatic signatures (*e.g.*, arc-related calc-alkaline rocks *vs* rift- or back-arc related alkaline-like lavas and/or exotic blocks from salt domes; see below).

Cadomian magmatic rocks are subalkaline to alkaline and compositionally bimodal, changing from basaltic to rhyolitic composition with few intermediate rocks, except for trachy-andesitic (high-K to shoshonitic) lavas from the Derik complex, southeast Anatolia (Figs. 3B–C and 5A–C). Mafic rocks seem to be rare in Turkey. The Cadomian magmatic rocks scatter widely in the low K tholeiitic to high K calc-alkaline-shoshonite series (Fig. 5B–D).

Mid-Oceanic Ridge Basalt (MORB)-normalized spider diagrams (Fig. 6) show that most Cadomian magmatic rocks (both mafic and felsic varieties) have typical arc signatures with enrichment in large ion lithophile elements (LILEs such as Rb, Ba, Sr) compared to high-field strength elements (HFSEs) and have negative Nb–Ta anomalies. Some of these rocks are enriched in light rare earth elements (LREEs) but not depleted in Nb–Ta and thus are similar to within-plate granites (for felsic rocks with zircon U–Pb ages of 526 ± 4 Ma and 535 ± 1.2, (Sepidbar et al., 2020; Shabanian et al., 2018)) and Enriched- Mid-Oceanic Ridge Basalts (*E*-MORBs) to Oceanic Island Basalts (OIB)-like rocks (for mafic rocks with zircon U–Pb ages of 539 ± 1.8 Ma, (Asadi Sarshar et al., 2020)). Felsic plutonic and volcanic rocks from Iran and

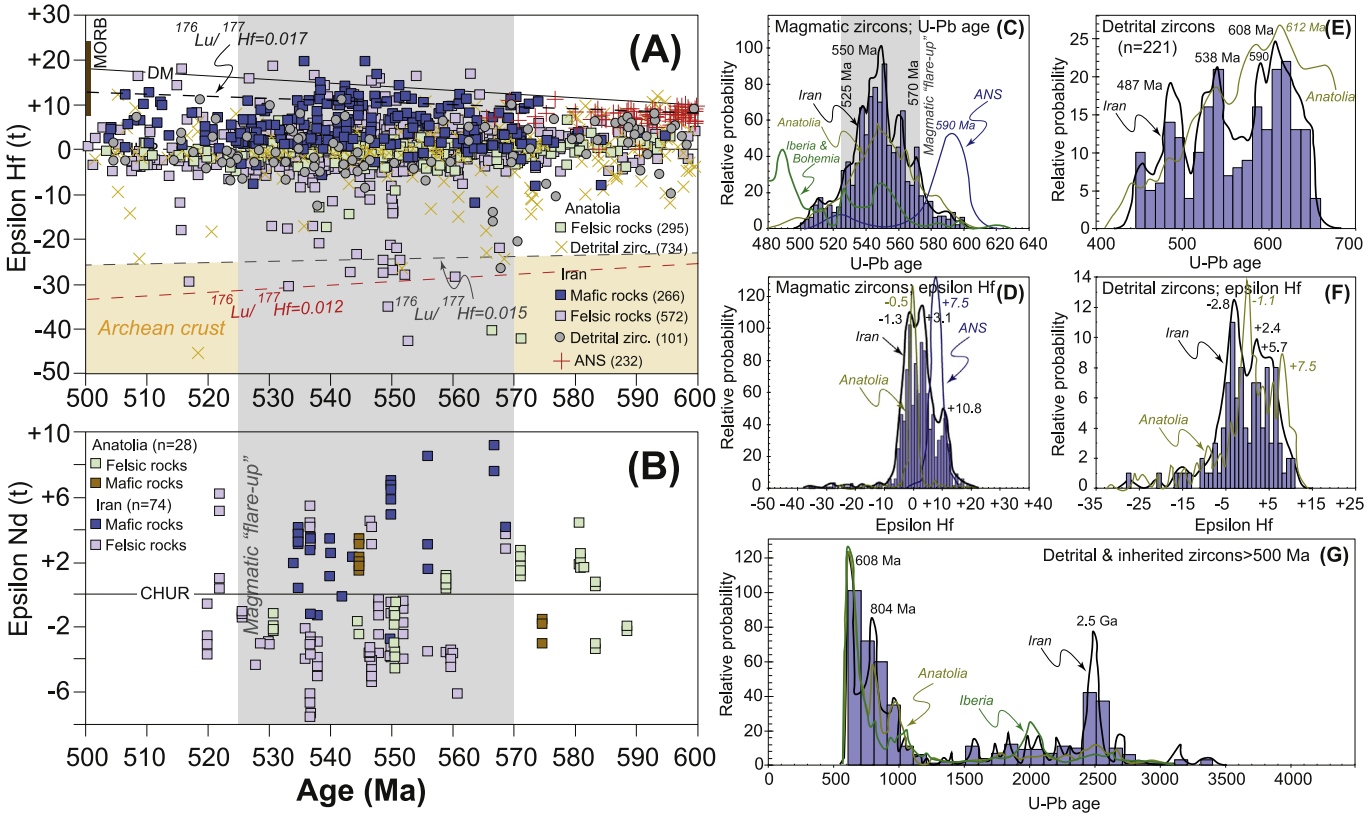

Fig. 4. Zircon Hf (A) and bulk-rock Nd (B) isotopes *vs* zircon $^{206}Pb/^{238}U$ age ($n = 2200$ zircon grains analysed for Lu–Hf isotope; $n = 102$ bulk rocks for Nd isotope; details about the analysed zircon grains are available in panel A) for Iran and Anatolia Cadomian mafic and felsic magmatic rocks (SiO_2 ranging from 50 to 70 *wt%*). For comparison, we show Hf-isotope data for detrital zircons from Iran and Anatolia as well as ANS magmatic zircons. $^{176}Lu/^{177}Hf$ values of 0.015, 0.012 and 0.017 are for an average continental crust, upper crust and mafic lower crust, respectively (Griffin et al., 2004). Probability diagrams for magmatic and detrital zircon $^{206}Pb/^{238}U$ ages of Iran and Anatolia (C and E), and for zircon Hf values (D and F). For comparison of we have plotted data from ANS, Iberia and Bohemia. A zircon age ($^{206}Pb/^{238}U$ for ages <1Ga and $^{207}Pb/^{235}U$ for ages >1Ga) plot of detrital and inherited zircons from Cadomian to Ordovician sediments and Cadomian magmatic rocks of Iran, Anatolia and Iberia (G). For references of compiled data, please see "Appendix A".

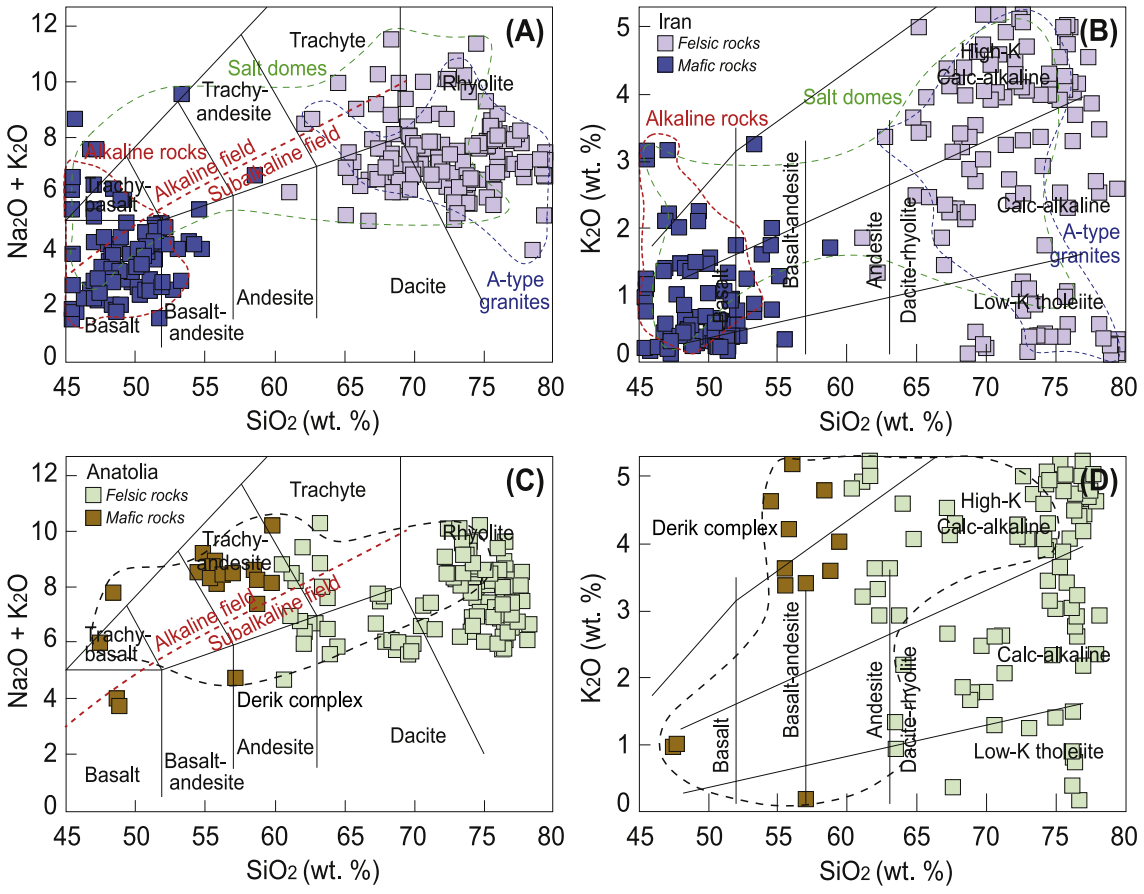

Fig. 5. (A) Total alkalis *vs* SiO_2 diagram after (Lebas et al., 1986) and (B) SiO_2 *vs* K_2O diagram for classification of the Iran-Anatolia Cadomian magmatic rocks. For references of compiled data, please see "Appendix A".

Anatolia have tendency to both volcanic-arc granites (VAG) and within-plate granites (WPG) in tectonic discrimination diagrams using Rb *vs* Y + Nb, Rb *vs* Yb + Ta, Nb *vs* Y and Ta *vs* Yb (Pearce et al., 1984) (Fig. 7). Once again, most Cadomian felsic rocks (>70%) are similar to volcanic arc granites (VAG), but some are more like within-plate granites (WPG).

Cadomian mafic rocks are sometimes similar to E-MORB and OIB (or basanites-hawaiites) and arc-related rocks in the Th/Yb *vs* Ta/Yb diagram (Pearce and Peate, 1995), whereas most felsic rocks are characterized by high Th/Yb ratios, although some (A-type granites) show similarities to OIB-like rocks (Fig. 8A). These differences can be attributed to a different contribution of continental crust to the felsic magmas; higher for arc-like granites and lower for A-type or OIB-like granites. A similar distinction is seen in the Nb/U *vs* Nb plot (Kepezhinskas et al., 1996); mafic rocks plot between OIBs and arc basalts (Fig. 8B), whereas most felsic rocks are characterized by low Nb/U and are similar to continental crust. Additionally, nearly all samples are characterized by low, non-adakitic $La/Yb_{(N)}$ and Sr/Y ratios and are similar to normal arc rocks (Fig. S1). Volcanic rocks from the Derik complex have higher $La/Yb_{(N)}$ ratio and Yb concentrations, similar to other shoshonites (Fig. S1).

3.3. Isotopic signatures of the magmatic pulses

Sr and Nd isotopes were analysed for new samples and integrated with data compiled from the literature. Initial εNd values were calculated using the available U–Pb zircon ages. Since $^{87}Sr/^{86}Sr$ initial ratios depend on $^{87}Rb/^{86}Sr$ ratios and can be erroneous for high $^{87}Rb/^{86}Sr$, data with $^{87}Rb/^{86}Sr > 4$ and $^{87}Sr/^{86}Sr_{(t)} < 0.700$ are not plotted in Fig. 9. For calculating the Nd model ages, we have used $^{147}Sm/^{144}Nd = 0.165$ as a cut-off.

Contemporaneous Cadomian mafic and felsic rocks from Iran have variable whole-rock εNd(t) ranging from +9 to −2.7 and + 6.1 to −7.7, respectively (Fig. 9). We have fewer whole-rock Nd isotopic data from Anatolia, but these show that Cadomian mafic and felsic rocks have εNd(t) from +3.2 to −3.1 and + 4.2 to −4.3, respectively (Table S3). Volcanic rocks from the Derik complex are similar; +3.2 to +0.5 (Gursu et al., 2015), but negative values (−1.2 to −2.3) are found in Cadomian granites of the Bitlis massif and metagranites (−0.5 to −4.3) and granulites (+1.4 to −3.6) of the Menderes massif (Ustaomer et al., 2009). In spite of overlapping ranges in initial Nd isotopic compositions, Cadomian mafic rocks are more mantle-like, whereas most felsic rocks have lower εNd(t), indicating a larger crustal contribution to the magmas (Fig. 9). Some mafic samples have εNd (t) values similar to that expected for MORB mantle (εNd(t) of +7.49 at 560 Ma) and show subduction-related geochemical fingerprints consistent with their emplacement in an arc setting. Mafic shoshonites from Derik may show derivation from a metasomatized sub-arc mantle, attested to by their shoshonitic signature with high contents of incompatible elements and by their isotopic signatures. The negative εNd(t) values of Cadomian felsic rocks also imply assimilation of older crust by mafic melts to generate the felsic outputs.

The Hf isotopic compositions of Cadomian magmatic zircons of Iran and Anatolia span a very wide range of εHf(t), from +20 to −43 (+20 to −43 for Iran, +16 to −43 for Anatolia) (Fig. 4A). Zircons in mafic rocks have a smaller range of εHf(t), from +20 to −25. Hf crustal model ages (T^C_{DM}) of the zircons with the least radiogenic Hf-isotope compositions vary between ~1 and 4 Ga, suggesting great heterogeneity in the pre-Cadomian crust beneath Iran and Anatolia.

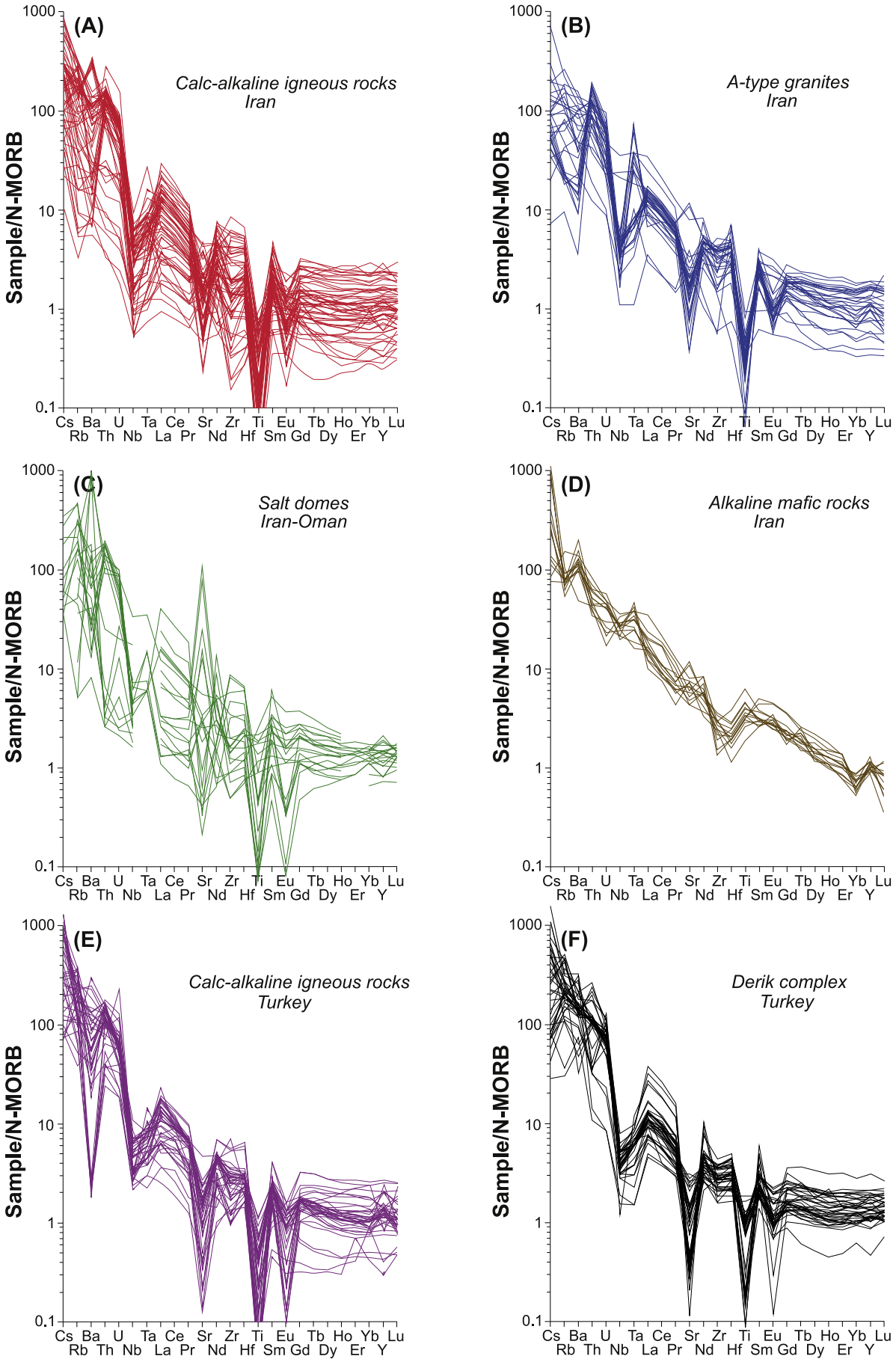
(A)
Calc-alkaline igneous rocks
Iran
(B)
A-type granites
Iran
(C)
Salt domes
Iran-Oman
(D)
Alkaline mafic rocks
Iran
(E)
Calc-alkaline igneous rocks
Turkey
(F)
Derik complex
Turkey
Sample/N-MORB
1000
100
10
1
0.1
Cs Ba U Ta Ce Sr Zr Ti Eu Tb Ho Yb Lu
Rb Th Nb La Pr Nd Hf Sm Gd Dy Er Y

4. Discussion

We use our new and compiled data to discuss four topics below: 1) Tempo and causes of Cadomian arc magmatism; 2) Geochemical and isotopic characteristics of Cadomian magmatic rocks; 3) Fractional crystallization and coupled assimilation-fractional crystallization processes in Cadomian magmatic evolution; and 4) Extensional tectonics, magmatic fronts and rear-arcs.

5. Tempo and causes of Cadomian arc magmatism

Cadomian magmatic activity in northern Gondwana was episodic, with evidence for a prolonged magmatic flare-up (Moghadam et al., 2017c). The compiled zircon U–Pb data indicate that Cadomian magmatism started at *ca* 620–600 Ma in Iran and Anatolia (Fig. 4C); these are the oldest rocks known from either region. Rates of magmatism climaxed at ~570 Ma, beginning with a ~ 45-Myr flare-up. The Iran-Anatolia flare-up resembles those observed in other continental arcs such as the Andes and the Gangdese arc in Tibet, but is significantly longer than the ~10–30 Myr episodes reported for Mesozoic-Cenozoic arcs (Ducea et al., 2017). The ages confirm that Iranian-Anatolian crust is related to the Cadomian magmatism of southern Europe, although the latter started earlier, at *ca* ~ 670 Ma (Linnemann et al., 2008). Detrital-zircon ages suggest a 542–525 Ma magmatic flare-up (with a peak at 538 Ma). The detrital zircon data suggest another magmatic climax at 620–580 Ma (with a peak at 608 Ma), which may reflect activity in the ANS (Fig. 4E).

Cadomian magmatism in Iran and Anatolia overlaps in time with ANS magmatism and sometimes the two episodes are linked together as "Pan-African", but ANS igneous activity is readily distinguished using combined age and Hf–Nd isotopic data. The ANS is characterized by voluminous 630–600 Ma calc-alkaline granites, evolving to increasingly alkaline intrusions between 610 and 570 Ma (Be'Eri-Shlevin et al., 2009; Morag et al., 2011). Furthermore, whole-rock εNd(t) and zircon εHf(t) of ANS igneous rocks are more radiogenic (Fig. 4A–D) suggesting that most ANS magmatism came from a depleted mantle without contamination by old continental crust. It may be more difficult to distinguish Iran-Anatolian Cadomian detrital zircons from those of the Saharan Metacraton because igneous rocks of these regions overlap in both age and isotopic composition (*e.g.*, (Meinhold et al., 2011)).

Considering the Cadomian exposures in Iran and Anatolia (and assuming a continental crust of ~30- km thick, see below) and our geochronological data, we suggest that the Cadomian crust of Iran and Anatolia formed at a rate of ~0.6 km^3/a (Moghadam et al., 2020a), which is a significant fraction of the modern global arc magma production rate of 1.65 km^3/a (Reymer and Schubert, 1984). This rate is also comparable to the rate of 0.78 km^3/a for the ANS during ~300 Myr of magmatism (Reymer and Schubert, 1984). The Cadomian crust of Iran and Anatolia was produced by ultrahigh magmatic addition rates of ~92,000 km^3/Myr during the flare-up stage (Moghadam et al., 2017c), a much higher rate than the ~40,000 km^3/Myr estimated for Phanerozoic North American arcs (Ducea et al., 2015). The causes of magmatic flare-up during the evolution of the Cadomian arcs are controversial. Cadomian magmatic arcs nucleated at *ca* ~ 670 Ma in southwest Europe and *ca* 620 Ma in Iran and Anatolia, with subduction of an old and dense Prototethyan oceanic lithosphere beneath Gondwana. Our data show that Cadomian arc magmatism was diachronous and formed in an extensional setting as indicated by thin continental crust (<30–40 km, (Moghadam et al., 2017c)), high magma fluxes over ~45 My and an abundance of Cadomian volcano-sedimentary basins. Thin Cadomian continental crust in Iran and Anatolia has been inferred using Sr/Y and La/Yb (Chapman et al., 2015) as well as Gd/Yb (Farner and Lee, 2017) ratios for intermediate rocks and Ce/Y ratios for mafic rocks (Mantle and Collins, 2008). (Chapman et al., 2015) suggested that the Sr/Y ratio can be used as a proxy for crustal thickness in intermediate calc-alkaline rocks (55–68 *wt*% SiO_2). Since Sr can be affected by plagioclase fractionation, we have also used the Gd/Yb and La/Yb ratios for our intermediate rocks (55–68% SiO_2). Our compiled data show that most Cadomian magmatic rocks with intermediate SiO_2 reflect a crustal thickness of 20 to 30 km (Moghadam et al., 2017c). Gabbroic rocks from Iran have maximum Ce/Y ratios <1.4, indicating a crustal thickness for the Iran Cadomian arc of <30 km (Moghadam et al., 2020a).

Extensional basins in Iran and Anatolia accumulated several kilometers of sediments along with retro-arc basins in the Cadomian of SW Europe (Nance et al., 2010) and other lines of evidence attest to this extension. Thin continental crust precludes the formation of thick-crust adakites, which are not known from the Cadomian magmatic rocks of Iran and Anatolia. It is suggested that continental extension - which ultimately led to the opening of the Rheic Ocean - triggered the 570–525 Ma magmatic flare-up, generating >90% of the continental crust of the region. This extension, perhaps accompanied by delamination of the metasomatized lower part of the lithospheric mantle, allowed upwelling and partial melting of the asthenosphere, and subsequent melting of the residual subcontinental lithospheric mantle and lower crust, generating mafic precursors for the magmatic flare-up. Such a scenario is consistent with the presence of Cadomian arc rocks that carry variable Nd–Hf isotope signatures of both juvenile mantle and reworked materials (Fig. 4A).

However, subduction and high melt production in Anatolia and Iran may have begun earlier (*e.g.*, (Nutman et al., 2014)), as the detrital-zircon dataset clearly shows a magmatic flare-up at 620–580 Ma. We suggest that Cadomian extension may reflect steepening of the proto-Tethyan slab and resulting trench roll-back. Slab rollback results in upper-plate extension and augmented arc magmatism such as that observed in Cordilleran subduction systems (Ducea et al., 2017). Trench roll-back is the most important cause of upper-plate extension and ultrahigh rates of magma generation in nearly all arcs worldwide (Ducea et al., 2017). It is most likely that similar roll-back of the subducting slab and the resultant upper plate extension triggered back-arc rifting, ultimately opening the Rheic Ocean (see next section). Waxing and waning of upper-plate extension from 620 to 500 Ma also explains the lack of Cadomian crustal thickening, and episodic magmatic flare-ups. Long-lived arcs with magmatic flare-ups can generate >30 km of ultramafic-mafic cumulates (Ducea et al., 2015); these are likely to be lost by delamination (Tilhac et al., 2016) and are rarely preserved in the Cadomian arcs, but are observed in the northeast Iran. High magmatic flux during the ~570–525 Ma extension probably triggered partial infiltration and accumulation of primary mafic magma in lower-crustal reservoirs which produced large volumes of magmatic cumulates such as those reported from northeast Iran with zircon U–Pb ages of 547–532 Ma (Moghadam et al., 2020a). These processes resulted in stratified Cadomian arc crust, with two pyroxene+olivine+amphibole (±garnet) mafic cumulates in the lower crust, mafic-felsic intrusions in the middle crust and volcano-sedimentary sequences in the upper crust. Delamination of arc-related dense cumulates and subsequent reactivation of the mantle wedge and related magmatism would produce the observed magmas with juvenile isotopic signatures. There is a connection between continental-arc tectonic regimes and cycles of magmatic flare-up *vs* lull. Some magmatic flare-ups are suggested to be related to upper plate compression during subduction,

Fig. 6. N-MORB-normalized trace-element patterns of Cadomian igneous rocks from Iran and Anatolia. Normalization data are from (Sun and McDonough, 1989). For references of compiled data, please see "Appendix A".

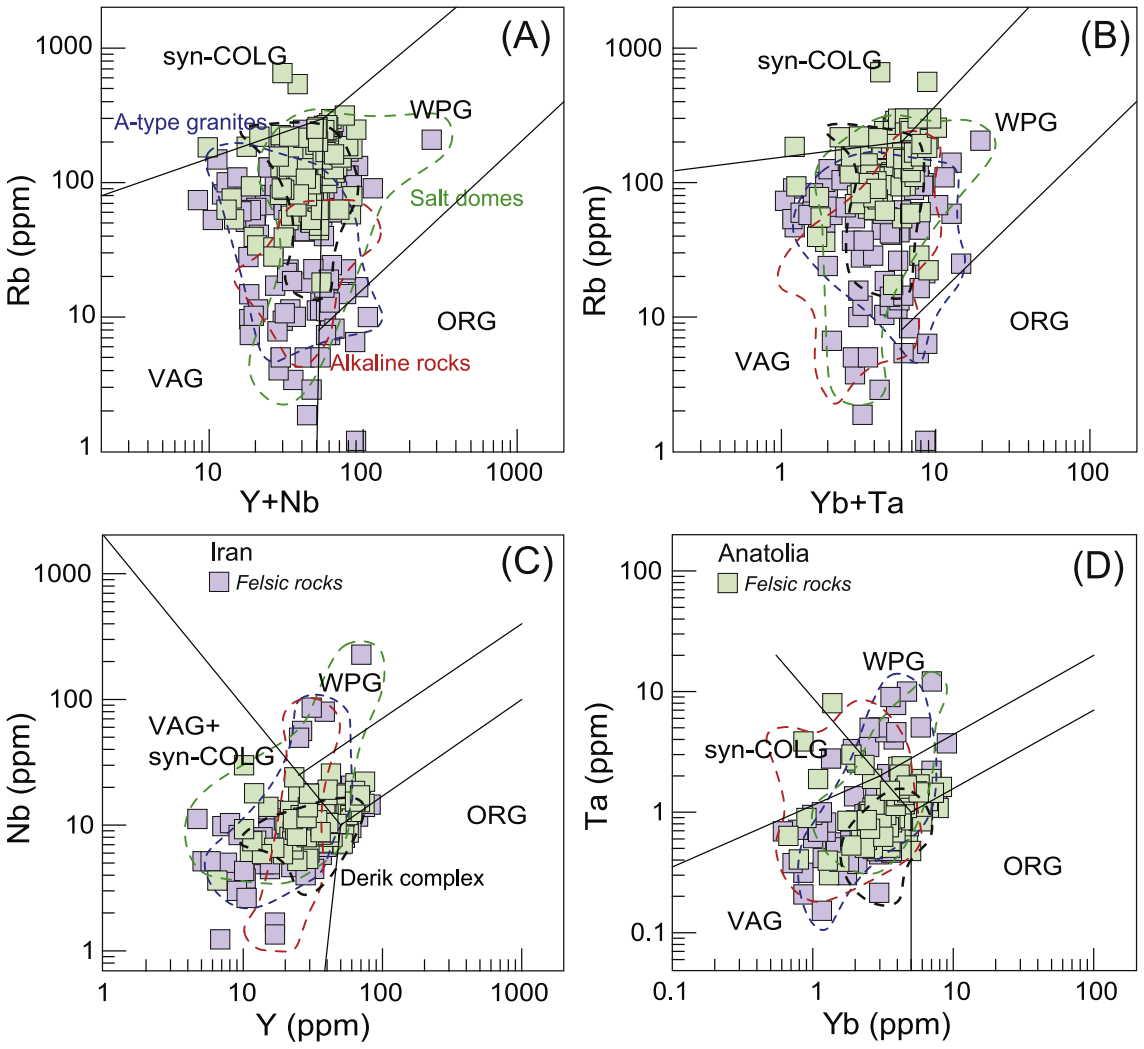

Fig. 7. Rb *vs* Y + Nb (A), Rb *vs* Yb + Ta (B), Nb *vs* Y (C) and Ta *vs* Yb (D) diagrams (Pearce et al., 1984) for classification of Cadomian felsic magmatic rocks from Iran and Anatolia (see caption Fig. 5 in "Appendix A" for references).

but the mechanism for this is difficult to understand. Recent studies on the Andean arc indicate there is also a relationship between the upper plate tectonic regime and the geometry of the subducting lithosphere.

In contrast to the Andean arcs, some fossilized arcs have evidence for extreme extension in the overlying plate - such as the Late Neoproterozoic-Early Cambrian arcs from north Gondwana - but similar to other arcs show traces of magmatic flare-up and isotopic perturbation in their magmatic rocks (Moghadam et al., 2017c). Magma productivity in these extensional arcs appears to be more continuous than in the compressional arcs. In these arcs, the extensional movements allow mantle and lower crust instabilities and cause high-degree melting of the sub-arc mantle, which play an important role in the generation of high magmatic fluxes.

Because crustal thickness controls the height of the mantle column available for melting beneath continental arcs (Plank and Langmuir, 1988), the extent of melting partly reflects the amount of adiabatic decompression, which is a function of melt-column length. Lithospheric thinning- such as that prevailed in the Cadomian territories- will lengthen the melt column beneath arcs, enhancing melting. The longer mantle column for arcs with thin continental crust will lead to higher degrees of mantle melting, which thus will generate flare-ups in the arc. In contrast, lithospheric thickening should lead to lulls because it shortens the melt column. Thermal runaway for triggering flare-up is less important in the extensional arcs. Nevertheless, thermal agents are important for assimilation and fractional-crystallization (AFC) and/or Melting, Assimilation, Storage and Homogenization (MASH) processes in the deep crust or crustal "hot zones".

6. Petrogenesis of Cadomian magmatic rocks

Compiled geochemical data from all Cadomian terranes show that >70% of the magmatic rocks have strong subduction-related geochemical signatures with negative anomalies in Nb–Ta and are similar to calc-alkaline volcanic-arc granitoids (Fig. 6). Shoshonitic rocks are also present and show subduction-related geochemical signatures but may have different sources than the calc-alkaline magmas. The arc-like Cadomian magmatic rocks have high concentrations of K, Rb, U, Th, Ba and other LILEs as well as LREEs, which are typical of continental-arc magmas. These geochemical characteristics imply a crustal contribution but depletion in Nb–Ta and other HFSEs relative to the LREEs, and enrichment of LILEs, may be related to fluids/melts released from the down-going slab and inducing mantle-wedge melting, or inherited from anatexis of the continental crust. Mafic shoshonites (absarokites) such as the Derik volcanic rocks can also originate from melting of a metasomatized sub-continental lithospheric mantle (SCLM) (Gursu et al., 2015). High-K felsic rocks are fractionated and their high concentrations of LILEs can be inherited from fractional crystallization (FC) and/or coupled assimilation-fractional crystallization (AFC) processes, which is

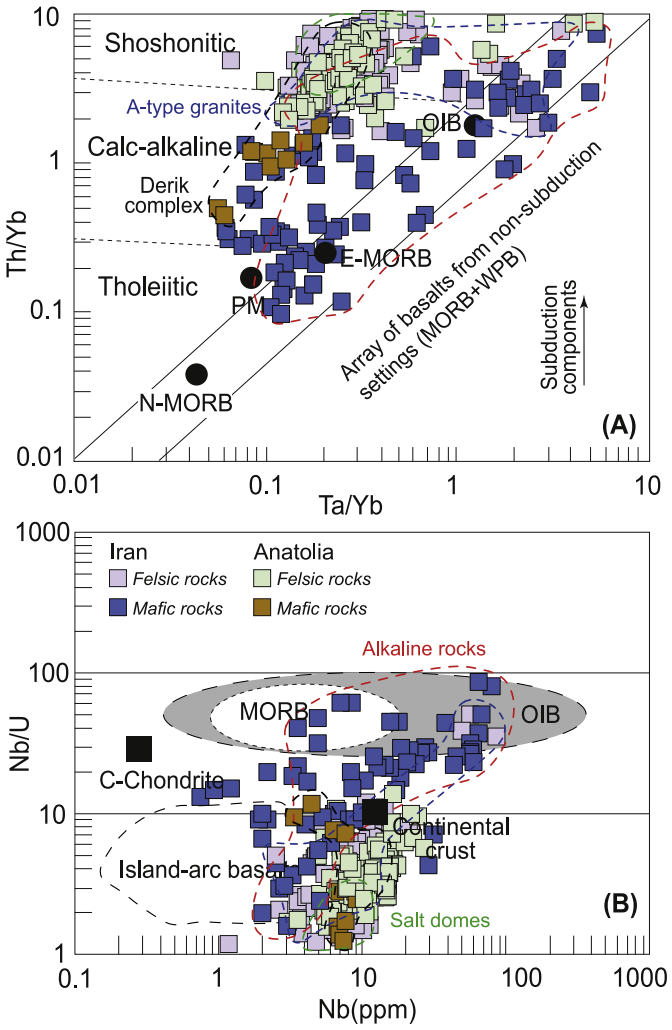

Fig. 8. (A) Th/Yb *vs* Ta/Yb (Pearce and Peate, 1995) and (B) Nb/U *vs* Nb (Kepezhinskas et al., 1996) for classification of Cadomian magmatic rocks from Iran and Anatolia (see caption Fig. 5 in "Appendix A" for references).

supported by their less radiogenic Nd-isotope values. A-type granites and mafic alkaline (basanites-hawaiites) or (*E*-MORB-) OIB-like rocks (both known from basement outcrops and/or as xenoliths within the Cadomian salt domes) should have a different source. Cadomian A-type granites can be generated from partial melting of lower-crustal amphibolites or granulites and/or by fractionation of mafic melts coming from partial melting of either a metasomatized sub-continental lithospheric mantle (SCLM) or from an asthenospheric mantle wedge (Sepidbar et al., 2020; Shabanian et al., 2018). The positive εNd(t) and εHf(t) values of the OIB-like mafic rocks, along with their enrichment in K, Rb, REEs and other HFSEs also suggest a mantle plume and/or a metasomatized mantle source such as SCLM for their formation, which is consistent with their genesis in a continental rift, including a continental back-arc basin (Sepidbar et al., 2020). Cadomian felsic rocks seem to be formed *via* extensive FC and AFC processes, which can be identified on the basis of εHf(t) and εNd(t) *vs* SiO_2 plots (see next section) where felsic rocks have less radiogenic Hf and Nd isotopes, reflecting the involvement of older crust. Since the geochemical and isotopic characteristics of Cadomian mafic and felsic rocks differ, we discuss their petrogenesis separately.

6.1. Zircon Lu–Hf isotopes

In addition to the variation in Nd isotopes of Cadomian magmatic rocks, data for Iranian magmatic zircons also show variable εHf (t) values with peaks at −1.3, +3.1 and + 10.8 (Fig. 4D). Furthermore, detrital (600–500 Ma) zircons are characterized by peaks at −2.8, +2.4 and + 5.7 (Fig. 4F). Cadomian detrital zircons from Anatolia have peaks at −1.1 and + 7.5. Although juvenile magmas clearly dominate, the large range in εHf(t) values can be explained by a threefold increase in magmatic flux during the ~45 Ma magmatic flare-up. The variable Hf-isotope values reflect a major contribution from older crust through combined assimilation-fractional crystallization (AFC) and melting-assimilation-storage-homogenization (MASH) processes, particularly in the felsic rocks, for which mafic magmas were probably thermal precursors.

We argue that two models can explain the observed Lu–Hf isotopic variations of Cadomian igneous rocks (Andersen et al., 2007; Miskovic and Schaltegger, 2009). The first involves melting of an isotopically heterogeneous reservoir (lower crust and/or upper mantle) which is consistent with the restricted range of $^{176}Hf/^{177}Hf$, as observed in Cadomian zircons with radiogenic Hf. The corresponding rocks were probably generated by fractional crystallization of melts derived from upper-mantle reservoirs that evolved with a $^{176}Lu/^{177}Hf$ ratio of ~0.017–0.019 (Fig. 4A), assuming a lack of garnet in the melt source. This is consistent with the low La/Yb and Sr/Y elemental ratios among analysed Cadomian magmatic rocks (Fig. S1), which imply their melts

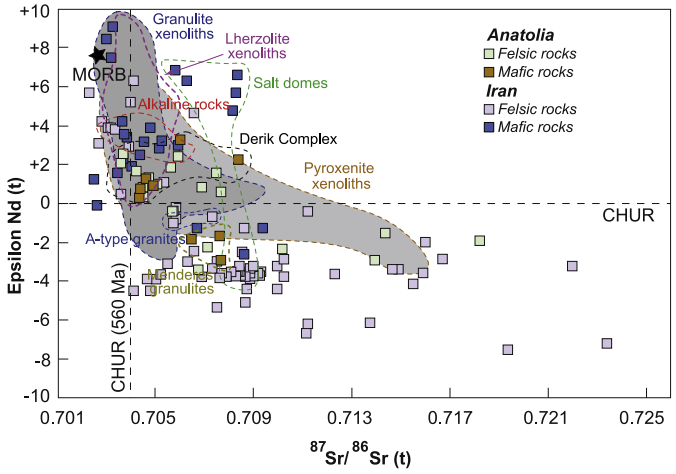

Fig. 9. Epsilon Nd *vs* $^{87}Sr/^{86}Sr$ (radiogenic growth corrected for 560 Ma) for Cadomian magmatic rocks of Iran and Anatolia (see Fig. 5 for references). Epsilon Nd (+7.74) and $^{87}Sr/^{86}Sr$ (0.702589) initial values for MORB are calculated using the present-day isotopic composition of N-MORBs, and assuming the Rb, Sr, Sm and Nd elemental concentrations by (Sun and McDonough, 1989). Data from pyroxenite, metasomatized lherzolite and granulite xenoliths are from (Griffin et al., 1988; O'Reilly and Griffin, 2013).

formed in a crust <~35 km thick (Moghadam et al., 2017c). However, it is worth noting that granulites and charnockites (with zircon U–Pb ages of 590–580 Ma; (Koralay, 2015)) are present in the Menderes massif and show that parts of the Cadomian crust may have been thicker than we expect.

The second model explains the Hf isotopic variability by a two-component mixing (Miskovic and Schaltegger, 2009) between a depleted-mantle melt (with present-day $^{176}Hf/^{177}Hf = 0.28328$ (Salters and Stracke, 2004), $^{176}Lu/^{177}Hf = 0.0384$ (Griffin et al., 2000) and 2.3 ppm Hf (Kelemen et al., 2003)) and older crust and sediments. The crustal components would have present-day $^{176}Hf/^{177}Hf = 0.28242$ and $^{176}Lu/^{177}Hf = 0.0008$ as inferred from the 2.5 Ga inherited zircons, assuming 5.1 ppm Hf (Gao et al., 1998)). In this model, the zircon Hf isotopic data can be replicated by assuming a 1.5–2.5 Ga crust, a $^{176}Lu/^{177}Hf$ ratio of 0.012–0.015 and 20–50% of crustal components. Such assimilation of old materials by the Cadomian magmas is also attested by the presence of xenocrystic zircons in nearly all analysed felsic igneous rocks. The incomplete assimilation and homogenization are also reflected in the range of zircon Hf isotopes within each sample.

The former existence of the older crust, which is not known from outcrops, is required as an assimilated component; this is supported by Nd–Hf model ages and by inherited zircons in magmatic rocks and detrital zircons in sediments. We therefore conclude that this older crust was essentially completely obliterated during the flare-up. Our compiled data for both inherited zircon cores in Cadomian igneous rocks and detrital zircons in Iran and Anatolia sediments show peaks at 0.6–0.8 Ga, 1.0 Ga, and 2.0–2.5 Ga (Fig. 4G), further suggesting either the presence of older crust or derivation of zircons from the interior of Greater Gondwana. The presence of a hidden crust beneath Iran and Anatolia, as old as Meso-Proterozoic (~1 Ga) to Paleo-Proterozoic and Paleo-Archean (2.4–3.6 Ga) also has been suggested based on xenocrystic zircons from the Cadomian magmayic rocks (Nutman et al., 2014). Moreover, our zircon Hf crustal model ages (T^C_{DM}) show many values of ~1 to 3.5 Ga (Fig. 10), which are consistent with the ages of inherited zircons. Iranian values of T^C_{DM} mostly are 1–2 Ga, whereas Anatolia is characterized by T^C_{DM} of 1–1.5 Ga. The Cadomian crust of Iberia differs in being dominated by inherited-zircon age peaks at 1 and 2 Ga (Fig. 4G), probably reflecting a less heterogenous crust or limited sampling.

6.2. FC-AFC modelling and Nd isotopes

We have discussed earlier -using both geochemical and isotopic data- that FC in deep crust formed mafic cumulates and the resultant ascending melts further suffered AFC in the mid-upper crust to generate the evolved felsic rocks, although a few felsic rocks have radiogenic Nd and Hf and do not have evidence for extensive assimilation of upper crustal materials. In this section, we simulate the FC-AFC processes using isotopic data and in particular the variation of $^{143}Nd/^{144}Nd_{(t)}$ with respect to SiO_2 (*wt%*) as a representative differentiation index. We use only the cogenetic, subduction-related rocks in our model (especially those have identical ages) and ignore the alkaline rocks (both lavas and rock clasts in salt diapirs) and A-type granites, since they have a different origin than I-type, subduction-related calc-alkaline rocks.

For the modelling, we used the selected equations of (DePaolo, 1981) and (Powell, 1984):

$$C_L = C_0{*}f + \left[\frac{r}{(r-1+D)}\right]{*}C_A{*}(1-f) \quad (1)$$

$$\varepsilon_L = \varepsilon_0 + (\varepsilon_A - \varepsilon_0){*}\left[1-\left(\frac{C_0}{C_L}\right){*}f\right] \quad (2)$$

$$f = F^{-\left(\frac{r+D-1}{r-1}\right)} \quad (3)$$

where i) C_0, C_A and C_L are the element concentrations in the parental magma, in the assimilant and in the daughter melt; ii) r is the ratio of the rate of assimilation relative to the rate of fractional crystallization; iii) D is the bulk partition coefficient; iv) F is the fraction of residual melt and v) e_0, e_A and e_L are the isotopic ratios (*e.g.*, $^{143}Nd/^{144}Nd$) in the parental magma, in the assimilant and in the residual melt.

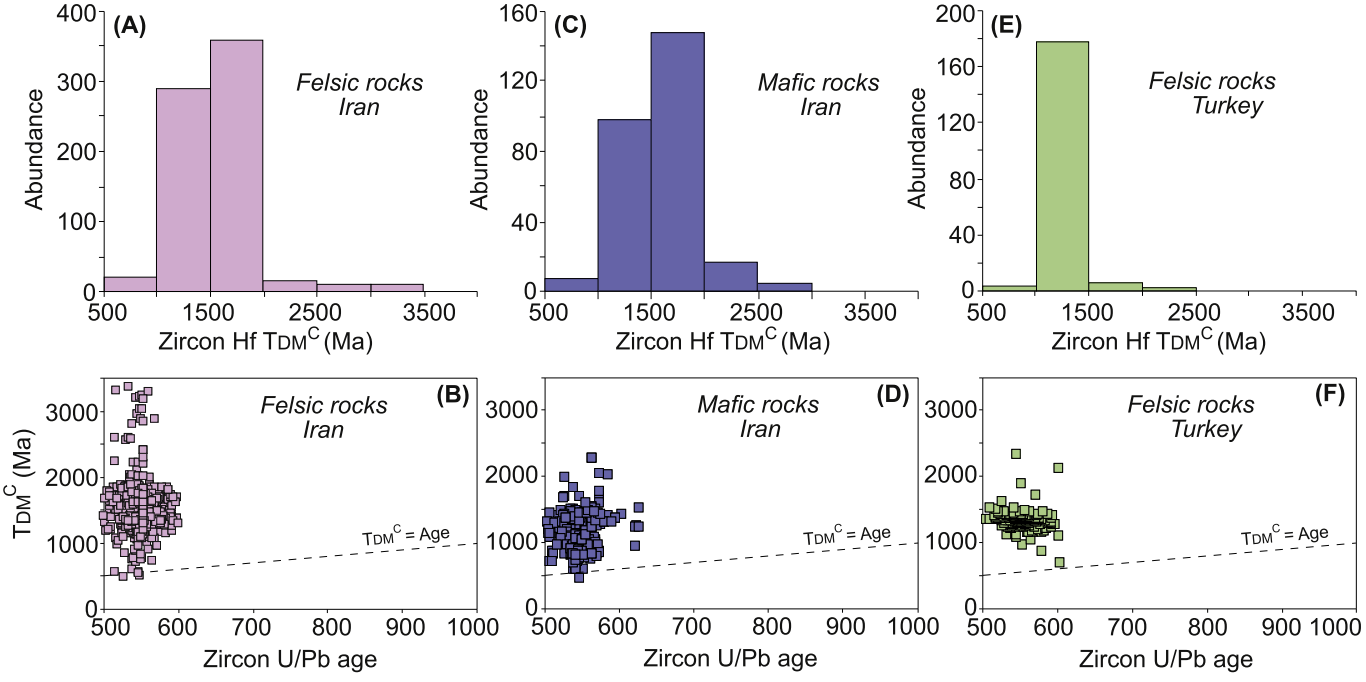

Fig. 10. Histograms for zircon crustal model ages (T^C_{DM}) and zircon T^C_{DM} *vs* crystallization ages for Cadomian magmatic pulses from Iran and Anatolia. References for zircon data are similar to caption Fig. 4 in "Appendix A".

In this study we consider the FC-AFC modelling using parameters and fractionating assemblages (*Ol model*: $Cpx_{2.6} + Pl_{40.8} + Ol_{54.9} + Ilm_{1.6}$ and *Hbl model*: $Cpx_{3.0} + Pl_{20.8} + Hbl_{74.5} + Ilm_{1.7}$) defined in (Moghadam et al., 2020a). The *Ol* and *Hbl* fractionating assemblages are considered to be representative of the clinopyroxene-bearing gabbro (cpx-gabbro) fractionation and of the amphibole-dominated fractionation of (Davidson et al., 2007), respectively, together with the gabbroic primary melts as starting melts and the Cadomian upper crust sedimentary rocks as assimilants. Phase/melt partition coefficients for basaltic-andesitic and dioritic melts were selected from the literature (*e.g.*, (Keshav et al., 2005; Vannucci et al., 1998), among others). Calculated partition coefficients (K_D) are i) for Ol model: $D_{Si} = 0.897$ and $D_{Nd} = 0.148$ and ii) for Hbl model: $D_{Si} = 0.941$ and $D_{Nd} = 3.419$. A complete description of the FC-AFC models and their parameters (*e.g.*, parental melts, assimilants, fractionating assemblages and partition coefficients), as applied to the Cadomian magmatic rocks from NE Iran, can be found in Appendix B of (Moghadam et al., 2020a).

Perfect fractional crystallization (Ol-FC and Hbl-FC curves in Fig. 12) indicates a melt evolution with negligible/limited crustal assimilation and is graphically represented by the lack of correlation between the Nd isotopes and SiO_2 (Fig. 11). The failure to correctly reproduce the main population of felsic rocks strongly suggests a contribution of crustal material during melt evolution. We suggest that the coupling of fractional crystallization (30–90%) and assimilation of felsic crust ($r = 0.2$) is able to describe the Nd-isotope signatures of the Iran and Anatolia Cadomian magmatism.

6.3. Source and genesis of Cadomian mafic rocks

Cadomian mafic rocks include calc-alkaline and alkaline suites. Alkaline mafic rocks occur as lavas and shallow plutonic bodies or dikes/sills within the Cadomian terrigenous sedimentary rocks in Central (Zarand) and northeast Iran (Torud) and/or as exotic blocks within the salt domes from southern Iran and northeast Oman. Shoshonitic mafic rocks (absarokites) occur in the Derik complex of southeast Anatolia. Nearly all these mafic rocks are fractionated and are characterized by Mg# (100 Mg/Mg + Fe) <50 and low Ni contents (except 3 samples, Fig. S2A). Fig. 11 shows that although these mafic rocks have different sources (different $^{143}Nd/^{144}Nd$ values at constant SiO_2), most also record significant crustal assimilation through AFC processes. Different sources for the genesis of these mafic rocks probably include the asthenosphere, which is geochemically equivalent to the depleted source of MORBs; SCLM which is assumed to develop its geochemical-isotopic complexities through metasomatic events; and OIB-type sources or mantle plumes, *i.e.*, enriched geochemical signatures coming from the deep mantle (650-km discontinuity). Melting of old SCLM, or other mantle volumes such as a mantle wedge that record interaction with metasomatic fluids/melts from deep mantle sources and/or from subducting plates can show more complexities (O'Reilly and Griffin, 1988; O'Reilly and Griffin, 2013). Contribution of OIB-type basanitic melts from the deep mantle can produce further heterogeneities in the SCLM (O'Reilly and Griffin, 1988). Crystallizing hydrous basaltic melts in the mantle can also generate pyroxenitic heterogeneities within the SCLM. Melting of a heterogenous SCLM (mica-amphibole-apatite lherzolites and/or pyroxenites) can generate melts with variable isotopic and geochemical signatures (Figs. 9 and 11).

Fig. 9 shows that some calc-alkaline mafic rocks may have originated from a depleted MORB-like source with radiogenic Nd isotope signatures and very young Nd depleted-mantle model (T_{DM}) ages (Fig. S2D). The Derik shoshonites and some calc-alkaline mafic rocks originated from an enriched source, similar to extremely subduction-modified SCLM (metasomatized lherzolites and/or pyroxenites, Fig. 9). This scenario is also supported by their old T_{DM} ages (1–1.5 Ga, Figs. S2D-E). Alkaline mafic rocks including mafic clasts from salt domes can have originated from an OIB-type source or from a modified SCLM metasomatized by basanitic melts. SCLM involvement is favored by lithospheric extension due to trench roll-back, and accompanying foundering of dense cumulates, which can be concomitant with a voluminous asthemosphere-related melt influx to the arc lithosphere. This can also lead to a return to juvenile isotopic compositions in some magmas and their zircons, with peaks in εHf(t) at +3.1 to +10.8. Mafic rocks with low εNd(t) and high $^{87}Sr/^{86}Sr$ record significant assimilation of old continental crust. Mafic clasts show high $^{87}Sr/^{86}Sr$ which can reflect the altered nature of these rocks.

The plots of incompatible-element ratios as well as $^{143}Nd/^{144}Nd$ and $^{87}Sr/^{86}Sr$ *vs* incompatible elements (Fig. 12) imply a heterogeneous mantle source for the mafic rocks as well as the assimilation of continental crust during the generation of evolved mafic rocks. In plots of $^{143}Nd/^{144}Nd$ and $^{87}Sr/^{86}Sr$ *vs* Sr/Nb and Zr/Nb, mafic rocks suggest melting of a metasomatized SCLM similar to lherzolite-pyroxenite xenoliths, although the Zr/Nb ratios attest to the contribution of another component, probably similar to global subducting sediments and/or continental crust (Fig. 12A–D). Plots of Th/Nb and K/Nb *vs* Zr/Nb also clearly show that two components were involved in the genesis of these rocks. One component comprises metasomatized mica-amphibole-apatite-bearing lherzolites and/or pyroxenites and the other component is similar to arc igneous rocks, subducting or continental sediments or even both. We suggest that a heterogenous SCLM with variable incorporation of different components from subducting slabs, including the

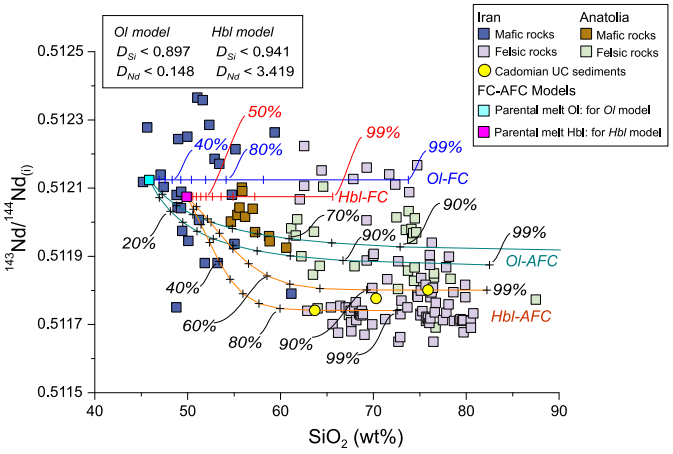

Fig. 11. Plot of initial, age corrected $^{143}Nd/^{144}Nd$ *vs* SiO_2 for Iran and Anatolia Cadomian magmatic rocks to modelise the FC and AFC processes (see text for explanation).

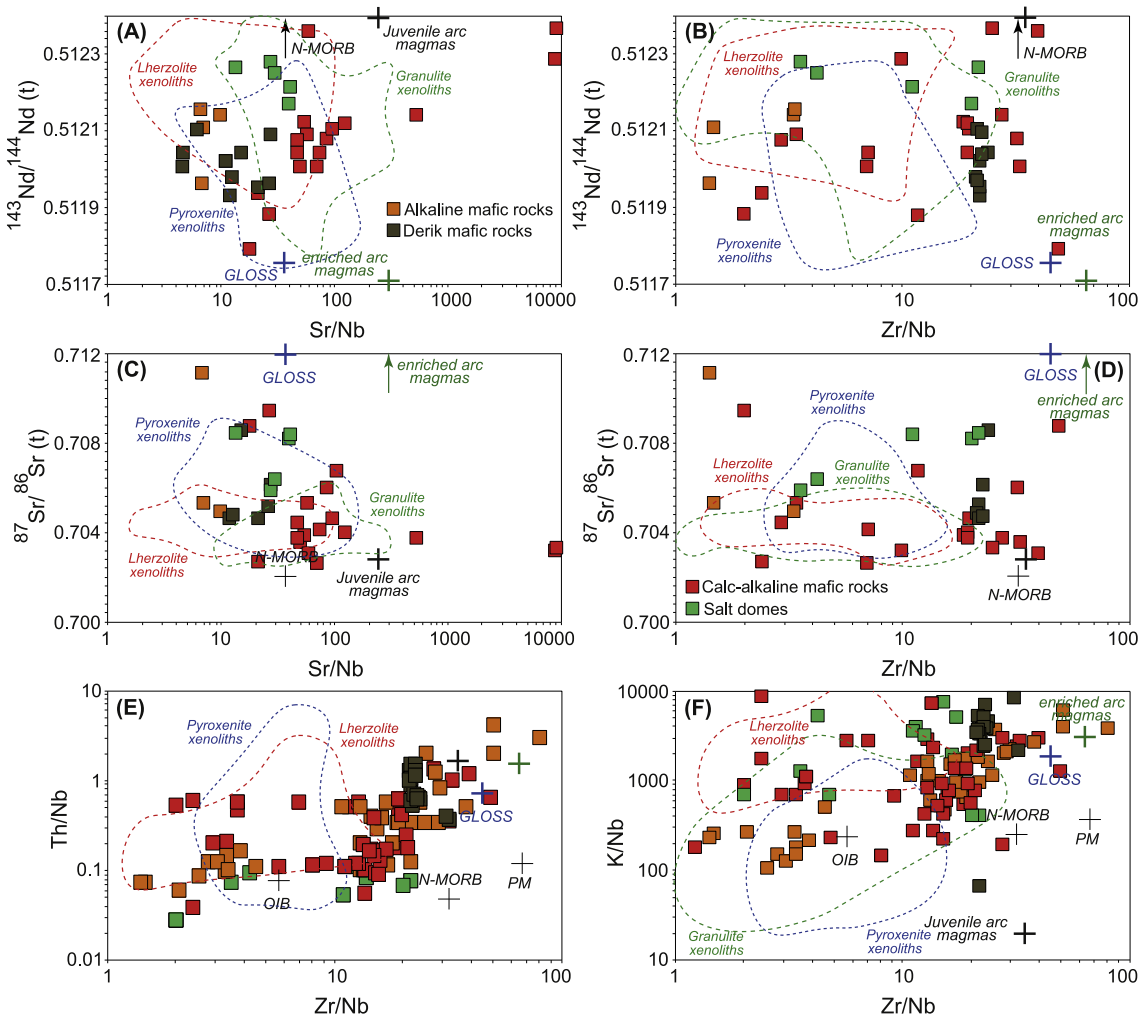

Fig. 12. Plots of $^{143}Nd/^{144}Nd$ *vs* Sr/Nb (A), $^{143}Nd/^{144}Nd$ *vs* Zr/Nb (B), $^{87}Sr/^{86}Sr$ *vs* Sr/Nb (C), $^{87}Sr/^{86}Sr$ *vs* Zr/Nb (D), Th/Nb *vs* Zr/Nb (E) and K/Nb *vs* Zr/Nb (F) for Cadomian mafic rocks of Iran and Anatolia. Compositions of primitive mantle (PM), normal mid-oceanic ridge basalts (N-MORB) and oceanic island basalts (OIB) are from (Sun and McDonough, 1989). Data from pyroxenite, metasomatized lherzolite and granulite xenoliths are from (Griffin et al., 1988; O'Reilly and Griffin, 2013). Enriched (high $^{87}Sr/^{86}Sr$ and low $^{143}Nd/^{144}Nd$) and juvenile (high $^{143}Nd/^{144}Nd$ and low $^{87}Sr/^{86}Sr$) arc magmas are from Urumieh-Dokhtar Cenozoic magmatic rocks of Iran (data from (Moghadam et al., 2020b)). The composition of global subducting sediments (GLOSS) is from (Plank and Langmuir, 1998).

sediment melts reflected in high Th/Nb and Zr/Nd ratios and their positive correlation, and/or involving basanitic melts from a deep mantle, can generate mantle sources for most of the Cadomian mafic rocks of Iran-Anatolia. The geochemical heterogeneities were accentuated during AFC processes in shallow-mantle and crustal magma chambers.

7. Extensional tectonics, magmatic fronts and rear-arcs

Above subduction zones, magmatic activity is concentrated along the magmatic front and behind it, in the "rear-arc" or "retro-arc". Some convergent margins have only a well-defined magmatic front and little rear-arc igneous activity. Extensional arcs such as the Cenozoic arcs in Iran have significant rear-arc magmatism (Moghadam et al., 2020b); this also is a dominant process at some active continental margins, such as the Andes, Cascades, and eastern Eurasia (*e.g.*, (Jacques et al., 2014)). Rifting of the Cadomian terranes from Gondwana during the Paleozoic complicates efforts to reconstruct the magmatic front *vs* retro-arc regions of the Anatolian-Iranian convergent margin. All studied Cadomian exposures from Iran, Anatolia and Iberia comprise both magmatic and sedimentary rocks (and/or their metamorphic equivalents, metamorphosed in greenschist to amphibolite facies) with minor eclogites, granulites and Cadomian ophiolites (Moghadam et al., 2017a; Ustaomer et al., 2009). The ratio of magmatic to sedimentary rocks varies from exposure to exposure. The high proportion of calc-alkaline plutonic rocks compared to volcanic rocks in Cadomian exposures may approximate the location of the main arc, *i.e.*, the magmatic front (Fig. 13). The volcanic rocks that may have been related to these exposures probably eroded extensively during Ediacaran-early Paleozoic and/or younger periods of uplift. The assumed magmatic front contains minor sediments, most of which are metamorphosed into greenschists and paragneisses. These rocks contain abundant 600–500 Ma old detrital zircons (~70–90%), with fewer (30–10%) older zircons. These sediments are interpreted as derived from the erosion of local Cadomian sedimentary, metamorphic and magmatic rocks and deposited in intra-arc basins. The maximum age of sedimentation is variable and overlaps in time with magmatic activity.

In contrast, some exposures include Cadomian sediments with minor volcanic rocks and might represent retro-arc regions. These exposures contain few plutonic rocks, but the volcanic rocks are interlayered with terrigenous sedimentary rocks as well as evaporites. The terrigenous sedimentary rocks (which mostly are unmetamorphosed) contain abundant Archean and Paleoproterozoic as well as Cadomian zircons, which show strong crustal reworking and a supply from both the juvenile crust of the Arabian-Nubian Shield and older cratons of Africa (Linnemann

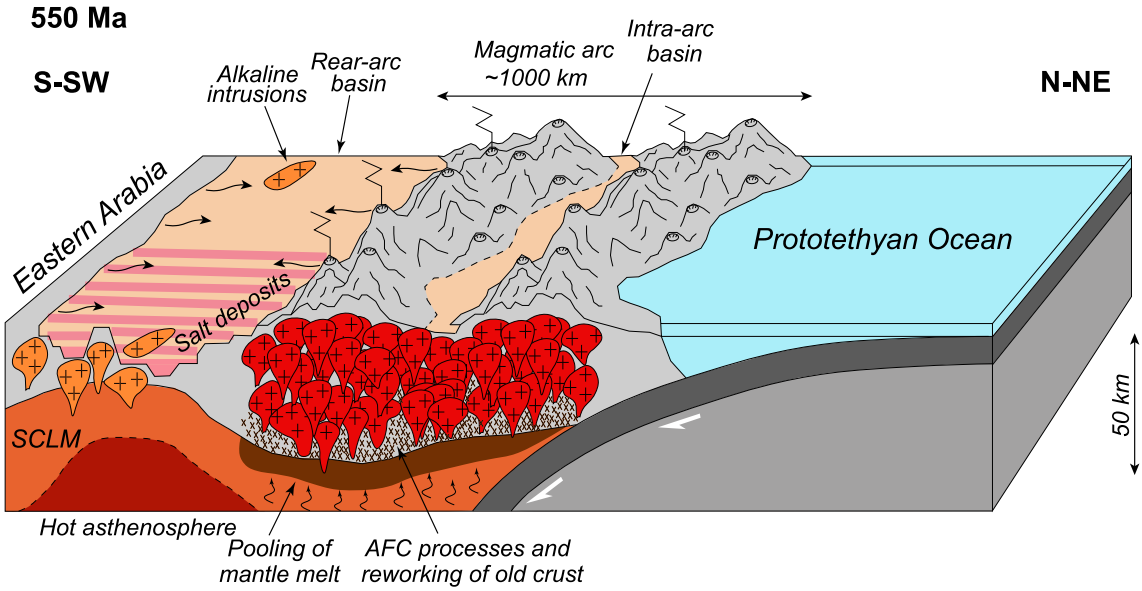

Fig. 13. Simplified cross-section of the Cadomian (~550 Ma) convergent margin of Northern Gondwana (Iran-Anatolia), showing magmatism along the main arc and rear-arc as well as detrital and evaporite sedimentation in the rear-arc.

et al., 2011; Moghadam et al., 2017b; Pereira et al., 2012). These sediments are suggested to be supplied from these regions *via* super-fan systems or detrital sheets (Meinhold et al., 2013). Archean and Paleoproterozoic xenocrystic zircons and/or zircon cores are also present in metasedimentary rocks (*e.g.*, paragneisses) from the Cadomian magmatic front, but the ratio of Cadomian to Archean-Paleoproterozoic zircons is much higher than in retro-arc sediments. The other important evidence for the existence of Cadomian retro-arcs is the occurrence of E-MORB to OIB-like mafic rocks, which are associated with thick sequences of terrigenous sediments as well as evaporites such as the dolomites near Zarand in central Iran, and/or accompanied by red sandstones and thick sequences of black dolomites, Na–K bearing salts, anhydrites and gypsum (Hormuz series) in salt domes from southwest Iran and northeast Oman.

Several scenarios have been suggested for the genesis of the OIB-like (basanites-hawaiites) mafic rocks (and coeval rhyolites, ignimbrites sandstones and evaporites) in Iran and Oman including formation in a retro-arc basin above a subduction zone, submarine volcanism in an extensional back-arc basin and formation in a continental, intra-plate rifts; all of these scenarios signify rift environments far from the main arcs. The presence of OIB-like rocks is important as indicating the location of continental extensional rifts, but the presence of similar-aged calc-alkaline and subduction-related rocks also implicates a convergent margin in the formation of these rocks. Therefore, the simultaneous presence of OIB-like and calc-alkaline magmatic rocks, terrigenous rocks and evaporites is most easily explained by a retro-arc environment for the genesis of these rocks (Bowring et al., 2007; Sepidbar et al., 2020; Thomas et al., 2015).

Extensional rifts are often found in back-arc regions of active continental margins and many of these are related to slab roll-back and ocean-ward retreat of the subduction hinge (Ducea et al., 2017). Slab roll-back is important because this causes upper-plate extension, crustal thinning, continental rifting and the addition of juvenile crustal (Miskovic and Schaltegger, 2009). In the case of the Cadomian convergent margin of Iran-Anatolia, extension and crustal thinning led to decompression melting of the SCLM beneath the retro-arc. Low degrees of melting of enriched SCLM and/or plume-influenced sub-arc mantle can generate the OIB-like melts we have documented. Such melts are not difficult to distinguish from OIBs from oceanic Islands and/or continental plumes, which are sometimes more undersaturated and isotopically evolved. Flux melting in the metasomatized sub-arc mantle beneath the retro-arc crust can also generate calc-alkaline mafic melts that can interact with overlying continental crust to produce I-type felsic rocks *via* assimilation and fractional crystallization.

8. Conclusions

Regional extension of a convergent margin on the northern flank of Gondwana caused a magmatic flare-up which produced most of the Cadomian crust now preserved in Iran-Anatolia. The presence of extensional basins in Iran and Anatolia that accumulated several kilometers of sediments along with mafic-felsic lavas and back-arc basin formation in the Cadomian of southwest Europe testifies to the importance of extension in the evolution of the Cadomian arc system in northern Gondwana. Trench roll-back was the most important cause of upper plate extension and caused ultrahigh rates of magma generation or flare-up in Iran and Anatolia. Cadomian mafic magmas were produced by decompression melting of SCLM followed by extensive fractionation and limited crustal assimilation. In contrast, Cadomian felsic rocks evolved from mafic parents that fractionated and assimilated more older crust through AFC and MASH processes during Cadomian arc magmatism. Alkaline rocks are also present in Cadomian terranes of Iran-Anatolia and are accompanied by thick sequences of detrital sedimentary rocks and/or occur as xenoliths in salt domes. Cadomian alkaline magmas reflect extension in back-arc or rear-arc basins established behind the main Cadomian arc.

Supplementary data to this article can be found online at https://doi.org/10.1016/j.lithos.2020.105940.

Declaration of Competing Interest

We hereby declare that: We have no pecuniary or other personal interest, direct or indirect, in any matter that raises or may raise a conflict of interest.

Acknowledgments

This study was funded by the “National Key Research and Development Program of China (2016YFE0203000)” and by “Chinese Academy of Sciences, President's International Fellowship Initiative

(PIFI, 2019VCB0013). Financial support was also received from the Alexander von Humboldt Foundation in the form of a senior research grant and GEOMAR Helmholtz Centre while preparing these results for publication. FL gratefully acknowledges the PRIN2017 Project 20177BX42Z_001 (Intraplate deformation, magmatism and topographic evolution of a diffuse collisional belt: Insights into the geodynamics of the Arabia-Eurasia collisional zones) and the grant to Department of Science, Roma Tre University (MIUR-Italy Dipartimenti di Eccellenza, ARTICOLO 1, COMMI 314 – 337 LEGGE 232/2016). We thank Semih Gürsu for providing us bulk rock data from Derik complex of Turkey. Zircon U–Pb geochronology and and Lu–Hf isotope data were obtained using instrumentation funded by DEST Systemic Infrastructure Grants, ARC LIEF, NCRIS/AuScope, industry partners, and Macquarie University. All logistical support for field studies came from Damghan University. This is contribution 1544 from the ARC Centre of Excellence for Core to Crust Fluid Systems (http://www.ccfs.mq.edu.au) and 1412 in the GEMOC Key Centre (http://www.gemoc.mq.edu.au), and 1380 from UTD Geosciences and is related to IGCP-662.

References

Abbo, A., Avigad, D., Gerdes, A., Gungor, T., 2015. Cadomian basement and Paleozoic to Triassic siliciclastics of the Taurides (Karacahisar dome, south-central Turkey): paleogeographic constraints from U-Pb-Hf in zircons. Lithos 227, 122–139.

Abdelsalam, M.G., Liégeois, J.-P., Stern, R.J., 2002. The saharan metacraton. J. Afr. Earth Sci. 34, 119–136.

Andersen, T., Griffin, W.L., Sylvester, A.G., 2007. Sveconorwegian crustal underplating in southwestern Fennoscandia: LAM-ICPMS U-Pb and Lu-Hf isotope evidence from granites and gneisses in Telemark, southern Norway. Lithos 93, 273–287.

Asadi Sarshar, M., Moghadam, H.S., Griffin, W.L., Santos, J.F., Stern, R.J., Ottley, C.J., Sarkarinejad, K., Sepidbar, F., O'Reilly, S.Y., 2020. Geochronology and geochemistry of exotic blocks of Cadomian crust from the salt diapirs of SE Zagros: the Chah-Banu example. Int. Geol. Rev. 1–22.

Avigad, D., Weissbrod, T., Gerdes, A., Zlatkin, O., Ireland, T.R., Morag, N., 2015. The detrital zircon U–Pb–Hf fingerprint of the northern Arabian–Nubian Shield as reflected by a Late Ediacaran arkosic wedge (Zenifim Formation; subsurface Israel). Precambrian Res. 266, 1–11.

Balaghi Einalou, M., Sadeghian, M., Zhai, M., Ghasemi, H., Mohajjel, M., 2014. Zircon U–Pb ages, Hf isotopes and geochemistry of the schists, gneisses and granites in Delbar Metamorphic-Igneous Complex, SE of Shahrood (Iran): Implications for Neoproterozoic geodynamic evolutions of Central Iran. J. Asian Earth Sci. 92, 92–124.

Be'Eri-Shlevin, Y., Katzir, Y., Whitehouse, M., 2009. Post-collisional tectonomagmatic evolution in the northern Arabian-Nubian Shield: time constraints from ion-probe U-Pb dating of zircon. J. Geol. Soc. Lond. 166, 71–85.

Beyarslan, M., Lın, Y.-C., Bingöl, A.F., Chung, S.-L., 2016. Zircon U-Pb age and geochemical constraints on the origin and tectonic implication of Cadomian (Ediacaran-early Cambrian) magmatism in SE Turkey. J. Asian Earth Sci. 130, 223–238.

Bowring, S.A., Grotzinger, J.P., Condon, D.J., Ramezani, J., Newall, M.J., Allen, P.A., 2007. Geochronologic constraints on the chronostratigraphic framework of the neoproterozoic Huqf Supergroup, Sultanate of Oman. Am. J. Sci. 307, 1097–1145.

Candan, O., Koralay, O., Topuz, G., Oberhänsli, R., Fritz, H., Collins, A., Chen, F., 2016. Late Neoproterozoic gabbro emplacement followed by early Cambrian eclogite-facies metamorphism in the Menderes Massif (W. Turkey): implications on the final assembly of Gondwana. Gondwana Res. 34, 158–173.

Chapman, J.B., Ducea, M.N., DeCelles, P.G., Profeta, L., 2015. Tracking changes in crustal thickness during orogenic evolution with Sr/Y: an example from the north American Cordillera. Geology 43, 919–922.

Davidson, J., Turner, S., Handley, H., Macpherson, C., Dosseto, A., 2007. Amphibole "sponge" in arc crust? Geology 35, 787–790.

DePaolo, D.J., 1981. A neodymium and strontium isotopic study of the Mesozoic calc-alkaline granitic batholiths of the Sierra Nevada and Peninsular Ranges, California. J. Geophys. Res. Solid Earth 86, 10470–10488.

Ducea, M.N., Barton, M.D., 2007. Igniting flare-up events in Cordilleran arcs. Geology 35, 1047–1050.

Ducea, M.N., Saleeby, J.B., Bergantz, G., 2015. The architecture, chemistry, and evolution of continental magmatic arcs. Annu. Rev. Earth Planet. Sci. 43 (43), 299–331.

Ducea, M.N., Bergantz, G.W., Crowley, J.L., Otamendi, J., 2017. Ultrafast magmatic buildup and diversification to produce continental crust during subduction. Geology 45, 235–238.

Erkül, S.T., Erkül, F., 2012. Petrogenesis of Pan-African metagranitoids in the central Menderes massif, Turkey: contribution of geochemical and Sr-Nd isotopic data to the study of source rock characteristics. 12th International Multidisciplinary Scientific Geoconference, SGEM 2012. 1, pp. 241–248.

Etemad-Saeed, N., Hosseini-Barzi, M., Adabi, M.H., Miller, N.R., Sadeghi, A., Houshmandzadeh, A., Stockli, D.F., 2015. Evidence for ca. 560Ma Ediacaran glaciation in the Kahar Formation, central Alborz Mountains, northern Iran. Gondwana Res. 31, 164–183.

Faramarzi, N.S., Amini, S., Schmitt, A.K., Hassanzadeh, J., Borg, G., McKeegan, K., Razavi, S.M.H., Mortazavi, S.M., 2015. Geochronology and geochemistry of rhyolites from Hormuz Island, southern Iran: a new record of Cadomian arc magmatism in the Hormuz Formation. Lithos 236, 203–211.

Farner, M.J., Lee, C.-T.A., 2017. Effects of crustal thickness on magmatic differentiation in subduction zone volcanism: a global study. Earth Planet. Sci. Lett. 470, 96–107.

Gao, S., Luo, T.C., Zhang, B.R., Zhang, H.F., Han, Y.W., Zhao, Z.D., Hu, Y.K., 1998. Chemical composition of the continental crust as revealed by studies in East China. Geochim. Cosmochim. Acta 62, 1959–1975.

Griffin, W., O'Reilly, S.Y., Stabel, A., 1988. Mantle metasomatism beneath western Victoria, Australia: II. Isotopic geochemistry of Cr-diopside lherzolites and Al-augite pyroxenites. Geochim. Cosmochim. Acta 52, 449–459.

Griffin, W.L., Pearson, N.J., Belousova, E., Jackson, S.E., van Achterbergh, E., O'Reilly, S.Y., Shee, S.R., 2000. The Hf isotope composition of cratonic mantle: LAM-MC-ICPMS analysis of zircon megacrysts in kimberlites. Geochim. Cosmochim. Acta 64, 133–147.

Griffin, W.L., Belousova, E.A., Shee, S.R., Pearson, N.J., O'Reilly, S.Y., 2004. Archean crustal evolution in the northern Yilgarn Craton: U-Pb and Hf-isotope evidence from detrital zircons. Precambrian Res. 131, 231–282.

Gursu, S., Moller, A., Goncuoglu, M.C., Koksal, S., Demircan, H., Koksal, F.T., Kozlu, H., Sunal, G., 2015. Neoproterozoic continental arc volcanism at the northern edge of the Arabian Plate, SE Turkey. Precambrian Res. 258, 208–233.

Jacques, G., Hoernle, K., Gill, J., Wehrmann, H., Bindeman, I., Lara, L.E., 2014. Geochemical variations in the Central Southern Volcanic Zone, Chile (38–43 S): the role of fluids in generating arc magmas. Chem. Geol. 371, 27–45.

Kelemen, P., Yogodzinski, G., Scholl, D., 2003. Along-strike variation in lavas of the Aleutian island arc: implications for the genesis of high Mg# andesite and the continental crust. Inside the Subduction Factory, Geophysical Monograph. 138, pp. 223–276.

Kepezhinskas, P., Defant, M.J., Drummond, M.S., 1996. Progressive enrichment of island arc mantle by melt-peridotite interaction inferred from Kamchatka xenoliths. Geochim. Cosmochim. Acta 60, 1217–1229.

Keshav, S., Corgne, A., Gudfinnsson, G.H., Bizimis, M., McDonough, W.F., Fei, Y., 2005. Kimberlite petrogenesis: Insights from clinopyroxene-melt partitioning experiments at 6 GPa in the CaO-MgO-Al2O3-SiO2-CO2 system. Geochim. Cosmochim. Acta 69, 2829–2845.

Koralay, O.E., 2015. Late Neoproterozoic granulite facies metamorphism in the Menderes Massif, Western Anatolia/Turkey: implication for the assembly of Gondwana. Geodin. Acta 27, 244–266.

Lebas, M.J., Lemaitre, R.W., Streckeisen, A., Zanettin, B., 1986. A chemical classification of volcanic rocks based on the total alkali silica diagram. J. Petrol. 27, 745–750.

Li, X.H., Abd El-Rahman, Y., Abu Anbar, M., Li, J., Ling, X.X., Wu, L.G., Masoud, A.E., 2018. Old continental crust underlying juvenile oceanic arc: evidence from northern Arabian-Nubian Shield, Egypt. Geophys. Res. Lett. 45, 3001–3008.

Linnemann, U., Pereira, F., Jeffries, T.E., Drost, K., Gerdes, A., 2008. The Cadomian Orogeny and the opening of the Rheic Ocean: the diacrony of geotectonic processes constrained by LA-ICP-MS U-Pb zircon dating (Ossa-Morena and Saxo-Thuringian zones, Iberian and Bohemian Massifs). Tectonophysics 461, 21–43.

Linnemann, U., Romer, R.L., Gerdes, A., Jeffries, T.E., Drost, K., Ulrich, J., 2010. The Cadomian orogeny in the Saxo–Thuringian zone. In: Linnemann, U., Romer, R.L. (Eds.), Pre–Mesozoic Geology of Saxo–Thuringia – From the Cadomian Active Margin to the Variscan Orogen. Schweizerbart, Stuttgart, pp. 37–58.

Linnemann, U., Ouzegane, K., Drareni, A., Hofmann, M., Becker, S., Gartner, A., Sagawe, A., 2011. Sands of West Gondwana: an archive of secular magmatism and plate interactions - a case study from the Cambro-Ordovician section of the Tassili Ouan Ahaggar (Algerian Sahara) using U-Pb-LA-ICP-MS detrital zircon ages. Lithos 123, 188–203.

Linnemann, U., Gerdes, A., Hofmann, M., Marko, L., 2014. The Cadomian Orogen: Neoproterozoic to early Cambrian crustal growth and orogenic zoning along the periphery of the West African Craton-Constraints from U-Pb zircon ages and Hf isotopes (Schwarzburg Antiform, Germany). Precambrian Res. 244, 236–278.

Mantle, G., Collins, W., 2008. Quantifying crustal thickness variations in evolving orogens: Correlation between arc basalt composition and Moho depth. Geology 36, 87–90.

Meinhold, G., Morton, A.C., Fanning, C.M., Frei, D., Howard, J.P., Phillips, R.J., Strogen, D., Whitham, A.G., 2011. Evidence from detrital zircons for recycling of Mesoproterozoic and Neoproterozoic crust recorded in Paleozoic and Mesozoic sandstones of southern Libya. Earth Planet. Sci. Lett. 312, 164–175.

Meinhold, G., Morton, A.C., Avigad, D., 2013. New insights into peri-Gondwana paleogeography and the Gondwana super-fan system from detrital zircon U–Pb ages. Gondwana Res. 23, 661–665.

Miskovic, A., Schaltegger, U., 2009. Crustal growth along a non-collisional cratonic margin: a Lu-Hf isotopic survey of the Eastern Cordilleran granitoids of Peru. Earth Planet. Sci. Lett. 279, 303–315.

Moghadam, H.S., Khademi, M., Hu, Z.C., Stern, R.J., Santos, J.F., Wu, Y.B., 2015. Cadomian (Ediacaran-Cambrian) arc magmatism in the ChahJam-Biarjmand metamorphic complex (Iran): magmatism along the northern active margin of Gondwana. Gondwana Res. 27, 439–452.

Moghadam, H.S., Griffin, W.L., Li, X.H., Santos, J.F., Karsli, O., Stern, R.J., Ghorbani, G., Gain, S., Murphy, R., O'Reilly, S.Y., 2017a. Crustal evolution of NW Iran: Cadomian arcs, Archean fragments and the Cenozoic magmatic flare-up. J. Petrol. 58, 2143–2190.

Moghadam, H.S., Li, X.H., Griffin, W.L., Stern, R.J., Thomsen, T.B., Meinhold, G., Aharipour, R., O'Reilly, S.Y., 2017b. Early Paleozoic tectonic reconstruction of Iran: tales from detrital zircon geochronology. Lithos 268, 87–101.

Moghadam, H.S., Li, X.H., Santos, J.F., Stern, R.J., Griffin, W.L., Ghorbani, G., Sarebani, N., 2017c. Neoproterozoic magmatic flare-up along the N. margin of Gondwana: the Taknar complex, NE Iran. Earth Planet. Sci. Lett. 474, 83–96.

Moghadam, H.S., Li, Q., Griffin, W., Stern, R., Ishizuka, O., Henry, H., Lucci, F., O'Reilly, S., Ghorbani, G., 2020a. Repeated magmatic buildup and deep "hot zones" in continental evolution: the Cadomian crust of Iran. Earth Planet. Sci. Lett. 531, 115989.

Moghadam, H.S., Li, Q.L., Li, X.H., Stern, R.J., Levresse, G., Santos, J.F., Lopez Martinez, M., Ducea, M.N., Ghorbani, G., Hassannezhad, A., 2020b. Neotethyan subduction ignited the Iran arc and Backarc differently. J. Geophys. Res. Solid Earth 125.

Mohseni, S., Aftabi, A., 2015. Structural, textural, geochemical and isotopic signatures of synglaciogenic Neoproterozoic banded iron formations (BIFs) at Bafq mining district (BMD), Central Iran: the possible Ediacaran missing link of BIFs in Tethyan metallogeny. Ore Geol. Rev. 71, 215–236.

Morag, N., Avigad, D., Gerdes, A., Belousova, E., Harlavan, Y., 2011. Crustal evolution and recycling in the northern Arabian-Nubian Shield: New perspectives from zircon Lu-Hf and U-Pb systematics. Precambrian Res. 186, 101–116.

Nance, R.D., Murphy, J.B., Keppie, J.D., 2002. A Cordilleran model for the evolution of Avalonia. Tectonophysics 352, 11–31.

Nance, R.D., Gutierrez-Alonso, G., Keppie, J.D., Linnemann, U., Murphy, J.B., Quesada, C., Strachan, R.A., Woodcock, N.H., 2010. Evolution of the Rheic ocean. Gondwana Res. 17, 194–222.

Nutman, A.P., Mohajjel, M., Bennett, V.C., Fergusson, C.L., 2014. Gondwanan Eoarchean-Neoproterozoic ancient crustal material in Iran and Turkey: zircon U-Pb-Hf isotopic evidence. Can. J. Earth Sci. 51, 272–285.

O'Reilly, S.Y., Griffin, W., 1988. Mantle metasomatism beneath western Victoria, Australia: I. Metasomatic processes in Cr-diopside lherzolites. Geochim. Cosmochim. Acta 52, 433–447.

O'Reilly, S.Y., Griffin, W., 2013. Mantle Metasomatism, Metasomatism and the Chemical Transformation of Rock. Springer, pp. 471–533.

Pearce, J.A., Peate, D.W., 1995. Tectonic implications of the composition of volcanic arc magmas. Annu. Rev. Earth Planet. Sci. 23, 251–285.

Pearce, J.A., Harris, N.B., Tindle, A.G., 1984. Trace element discrimination diagrams for the tectonic interpretation of granitic rocks. J. Petrol. 25, 956–983.

Pereira, M.F., Linnemann, U., Hofmann, M., Chichorro, M., Sola, A.R., Medina, J., Silva, J.B., 2012. The provenance of Late Ediacaran and Early Ordovician siliciclastic rocks in the Southwest Central Iberian Zone: constraints from detrital zircon data on northern Gondwana margin evolution during the late Neoproterozoic. Precambrian Res. 192-95, 166–189.

Plank, T., Langmuir, C.H., 1988. An evaluation of the global variations in the major element chemistry of arc basalts. Earth Planet. Sci. Lett. 90, 349–370.

Plank, T., Langmuir, C.H., 1998. The chemical composition of subducting sediment and its consequences for the crust and mantle. Chem. Geol. 145, 325–394.

Powell, R., 1984. Inversion of the assimilation and fractional crystallization (AFC) equations; characterization of contaminants from isotope and trace element relationships in volcanic suites. J. Geol. Soc. Lond. 141, 447–452.

Pu, J.P., Bowring, S.A., Ramezani, J., Myrow, P., Raub, T.D., Landing, E., Mills, A., Hodgin, E., Macdonald, F.A., 2016. Dodging snowballs: geochronology of the Gaskiers glaciation and the first appearance of the Ediacaran biota. Geology 44, 955–958.

Ramezani, J., Tucker, R.D., 2003. The Saghand Region, Central Iran: U-Pb geochronology, petrogenesis and implications for Gondwana Tectonics. Am. J. Sci. 303, 622–665.

von Raumer, J.F., Stampfli, G.M., Borel, G., Bussy, F., 2002. Organization of pre-Variscan basement areas at the north-Gondwanan margin. Int. J. Earth Sci. 91, 35–52.

von Raumer, J.F., Stampfli, G.M., Arenas, R., Martinez, S.S., 2015. Ediacaran to Cambrian oceanic rocks of the Gondwana margin and their tectonic interpretation. Int. J. Earth Sci. 104, 1107–1121.

Reymer, A., Schubert, G., 1984. Phanerozoic addition rates to the continental-crust and crustal growth. Tectonics 3, 63–77.

Saki, A., Moazzen, M., Oberhansli, R., 2011. P-T evolution of the precambrian metamorphic complex, NW Iran: a study of metapelitic rocks. Geol. J. 46, 10–25.

Salters, V.J., Stracke, A., 2004. Composition of the depleted mantle. Geochem. Geophys. Geosyst. 5.

Sepidbar, F., Shafaii Moghadam, H., Li, C., Stern, R.J., Jiantang, P., Vesali, Y., 2020. Cadomian magmatic rocks from Zarand (SE Iran) formed in a Retro-arc basin. Lithos 366–367.

Shabanian, N., Davoudian, A.R., Dong, Y.P., Liu, X.M., 2018. U-Pb zircon dating, geochemistry and Sr-Nd-Pb isotopic ratios from Azna-Dorud Cadomian metagranites, Sanandaj-Sirjan Zone of western Iran. Precambrian Res. 306, 41–60.

Shahzeidi, M., Moayyed, M., Murata, M., Yui, T.-F., Arai, S., Chen, F., Pirnia, T., Ahmadian, J., 2017. Late Ediacaran crustal thickening in Iran: Geochemical and isotopic constraints from the~ 550 Ma Mishu granitoids (Northwest Iran). Int. Geol. Rev. 59, 793–811.

Stern, R.J., Johnson, P., 2010. Continental lithosphere of the Arabian Plate: a geologic, petrologic, and geophysical synthesis. Earth Sci. Rev. 101, 29–67.

Stosch, H.G., Romer, R.L., Daliran, F., Rhede, D., 2011. Uranium-lead ages of apatite from iron oxide ores of the Bafq District, East-Central Iran. Mineral. Deposita 46, 9–21.

Sun, S.-S., McDonough, W.-S., 1989. Chemical and isotopic systematics of oceanic basalts: implications for mantle composition and processes. Geol. Soc. Lond. Spec. Publ. 42, 313–345.

Thomas, R.J., Ellison, R.A., Goodenough, K.M., Roberts, N.M.W., Allen, P.A., 2015. Salt domes of the UAE and Oman: probing eastern Arabia. Precambrian Res. 256, 1–16.

Tilhac, R., Ceuleneer, G., Griffin, W.L., O'Reilly, S.Y., Pearson, N.J., Benoit, M., Henry, H., Girardeau, J., Grégoire, M., 2016. Primitive arc magmatism and delamination: petrology and geochemistry of pyroxenites from the cabo ortegal complex, Spain. J. Petrol. 57, 1921–1954.

Tilhac, R., Grégoire, M., O'Reilly, S.Y., Griffin, W.L., Henry, H., Ceuleneer, G., 2017. Sources and timing of pyroxenite formation in the sub-arc mantle: Case study of the Cabo Ortegal Complex, Spain. Earth Planet. Sci. Lett. 474, 490–502.

Topuz, G., Gocmengil, G., Rolland, Y., Celik, O.F., Zack, T., Schmitt, A.K., 2013. Jurassic accretionary complex and ophiolite from northeast Turkey: no evidence for the Cimmerian continental ribbon. Geology 41, 255–258.

Triantafyllou, A., Berger, J., Baele, J.-M., Mattielli, N., Ducea, M.N., Sterckx, S., Samson, S., Hodel, F., Ennih, N., 2020. Episodic magmatism during the growth of a Neoproterozoic oceanic arc (Anti-Atlas, Morocco). Precambrian Res. 339, 105610.

Ustaomer, P.A., Ustaomer, T., Collins, A.S., Robertson, A.H.F., 2009. Cadomian (Ediacaran-Cambrian) arc magmatism in the Bitlis Massif, SE Turkey: magmatism along the developing northern margin of Gondwana. Tectonophysics 473, 99–112.

Vannucci, R., Bottazzi, P., Wulff-Pedersen, E., Neumann, E.-R., 1998. Partitioning of REE, Y, Sr, Zr and Ti between clinopyroxene and silicate melts in the mantle under La Palma (Canary Islands): implications for the nature of the metasomatic agents. Earth Planet. Sci. Lett. 158, 39–51.